AD-A272 065

OCUMENTATION PAGE

Form Approved
OMB No. 0704-0188

2. REPORT DATE	3. REPORT TYPE AND DATES COVERED
05-31-93	Final - 09-30-92 to 03-30-93

4. TITLE AND SUBTITLE
Novel N x N Integrated Channel Waveguide Optical Crossbars for Large Scale High Speed Non-Blocking Data Switching

5. FUNDING NUMBERS
C-F49620-92-C-0076

6. AUTHOR(S)
Michael Wang, Ph.D.

AFOSR-TR- 93 0413

7. PERFORMING ORGANIZATION NAME(S) AND ADDRESS(ES)
Physical Optics Corporation
20600 Gramercy Place, Building 100
Torrance, California 90501

DTIC ELECTE NOV 03 1993 S A D

8. PERFORMING ORGANIZATION REPORT NUMBER
3188-Final

9. SPONSORING / MONITORING AGENCY NAME(S) AND ADDRESS
Air Force of Scientific Research
Building 410
Bolling Air Force Base, D.C. 20332-6448

10. SPONSORING / MONITORING AGENCY REPORT NUMBER
0002AA Final Technical Report
1602/01

11. SUPPLEMENTARY NOTES

12a. DISTRIBUTION / AVAILABILITY STATEMENT
The United States Government is authorized to reproduce and distribute reprints for governmental purposes notwithstanding any copyright notation hereon.

12b. DISTRIBUTION CODE
This document has been approved for public release and sale; its distribution is unlimited.

13. ABSTRACT *(Maximum 200 words)*

Physical Optics Corporation proposed a new structure for an optical crossbar based on a multi-wavelength ring resonator tuning/switching. To demonstrate its feasibility, in Phase I, we designed, analyzed, and demonstrated a basic ring resonator tuning/switching element for the crossbar. Two approaches for ring resonator tuning were identified: fiber-based ring resonator and waveguide-based ring resonator. For simplicity of the Phase I concept demonstration, we demonstrated a fiber ring resonator. At HeNe laser wavelengths of 632.8 and 611.9 nm, the fiber resonator demonstrated the desired wavelength selective switching operation. The finesse of the present unoptimized device was measured at about 19 under zero tap coupling, with a potential of exceeding 100. The device provided over 36% throughput with a potential for throughput efficiency of over 80%. The crosstalk was measured at -8 dB with a potential of better than -33 dB. Optimization is possible by reducing the coupler loss. Waveguide fabrication and fiber/waveguide pigtailing experiments were also conducted in Phase I to demonstrate pigtailing capability for crossbar applications.

93-14523

14. SUBJECT TERMS
Optical Crossbar Switch, Ring Resonator, Wavelength Selective, Electrooptic

15. NUMBER OF PAGES
57

16. PRICE CODE

17. SECURITY CLASSIFICATION OF REPORT	18. SECURITY CLASSIFICATION OF THIS PAGE	19. SECURITY CLASSIFICATION OF ABSTRACT	20. LIMITATION OF ABSTRACT
Unclassified	Unclassified	Unclassified	SAR

DISCLAIMER NOTICE

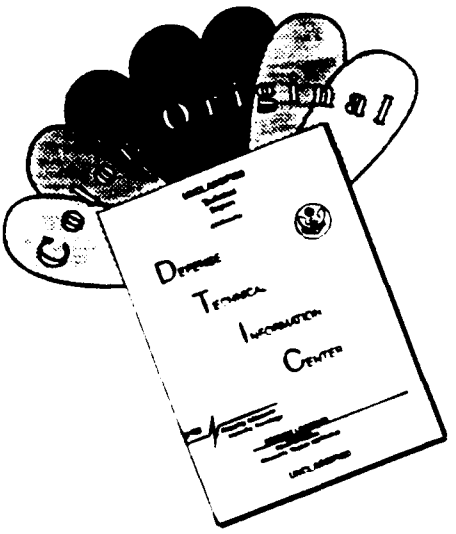

THIS DOCUMENT IS BEST QUALITY AVAILABLE. THE COPY FURNISHED TO DTIC CONTAINED A SIGNIFICANT NUMBER OF COLOR PAGES WHICH DO NOT REPRODUCE LEGIBLY ON BLACK AND WHITE MICROFICHE.

Novel N x N Integrated Channel Waveguide Optical Crossbars for Large Scale High Speed Non-Blocking Data Switching

Final Report

Contract No. F49620-92-C-0076

Period of Performance: 09/30/92 to 03/30/93

Presented to:

Air Force Office of Scientific Research
Directorate of Physics and Electronics
Building 410
Bolling AFB, DC 20332-6448

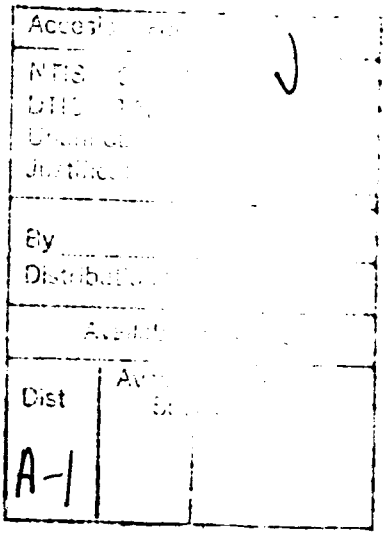

Presented by:

Physical Optics Corporation
20600 Gramercy Place, Suite 103
Torrance, California 90501
(310) 320-3088

Principal Investigator:
Dr. Michael Wang

May 1993

Research sponsored by the Air Force Office of Scientific Research (AFMC), under Contract F49620-92-C-0076. The United States Government is authorized to reproduce and distribute reprints for governmental purposes notwithstanding any copyright notation hereon.

TABLE OF CONTENTS

1.0 INTRODUCTION

Optical signal switching with the use of crossbar switching arrays is necessary in systems that rely on the transmission and processing of optical signals, such as in optical computing, optical interconnects, long-haul optical communications, and local area networks. Each application of optical crossbar switches imposes slightly different requirements on the performance of the switching network. Communication networks require low insertion loss, high data bandwidth, small crosstalk, fast switching speed, and compatibility of the interface with the optical fibers. Highly parallel interconnection networks for computing systems give more weight to the flexibility of the array size and interconnect architecture, that is, to switching pattern reconfigurability. The primary advantage of photonic crossbar switching is its capability to handle very wide band signals while fulfilling all other requirements.

Currently, optical crossbar switches require at least N^2 switching elements to perform N x N switching. To handle a large number of channels with high throughput and minimal crosstalk, such crossbar devices are difficult to realize because of the limitations of current switching device architectures and fabrication technologies. For example, the fiber optic PLZT crossbar, developed by Optivision [1], can work at gigahertz data rate and is capable of interconnecting M input fibers to N output fibers with an arbitrary interconnection pattern. However, to achieve high ON-OFF contrast ratio and low transmission loss, it requires a very high half-wave voltage (up to 200 volts). This limits the configuration time of the switch to about 20 μs and increases the system power dissipation. Furthermore, it requires a large number of fiber splitters (2N) and lenses ($2N^2$) for an N x N network; the result is a very bulky switching device.

An integrated optical crossbar technology has better compactness and ruggedness. It is based primarily on the electro-optic switch array [2,3] and on $LiNbO_3$ waveguides. To achieve non-blocking characteristics, N^2 switches are also required in an N x N switching network. Despite excellent high-speed (~nsec) element switching and relatively small device size, the number of channels is strongly limited by crosstalk (including electrical signal crosstalk) accumulated in the system at each switching element. Some state-of-the-art integrated crossbars have demonstrated 8 x 8 switching [4]; however, fiber/waveguide pigtailing is required for these devices to be useful for fiber optic communication.

Both bulk and integrated devices need at least a N^2 switching element for the N x N crossbar switch. The system crosstalk level can easily be accumulated through the large number of switch elements. Furthermore, the reconfiguration circuits are quite complex since under non-blocking

conditions the change of one pathway may affect the other pathways. The status of the many switch elements must be changed according to a calculated non-blocking switching pattern. Thus, reconfiguration rate (not element switching rate) will be slow; this is in addition to the crosstalk disadvantage just mentioned. The needs for high speed reconfiguration, low crosstalk, fiber interfacability, and multi-wavelength applicability call on the need for a new device structure for the crossbar switch.

The Phase I research, as proposed by Physical Optics Corporation (POC), was essentially a feasibility study of a new device architecture for optical crossbars. The architectures of the fiber-based crossbar and the waveguide-based crossbar are depicted in Figures 1-1 and 1-2, respectively. They both utilize ring resonator switches to perform highly wavelength-selective switchings. Only 2N switching elements are obviously needed for such crossbar structures. The accomplishment of Phase I work can be summarized as follows.

(1) We studied the principle of the crossbar switch structure. Theoretical results were positive, showing that the proposed device structure is experimentally feasible.

(2) The fiber ring resonator, as a fundamental building block of the fiber-based crossbar, was constructed to experimentally demonstrate the feasibility of the crossbar concept. This fiber-based crossbar can find an immediate application in fiber communication networks without additional interface effort and it has the potential for near-term commercialization despite its bulkiness.

(3) The waveguide bending and propagation loss was identified in Phase I as the fundamental issue that will limit the performance of the waveguide-based crossbar. The low loss waveguide device has yet to be demonstrated for ring crossbar applications.

Emphasizing the waveguide ring device in Phase I, as originally planned, would have focused our research on low loss waveguide fabrication. This was found to be unrealistic due to the time constraints of the Phase I program. It obviously would de-emphasize the major program goal of demonstrating the feasibility of the new crossbar concept. Hence, in consultation with the program monitor, the waveguide based ring device study was changed to the above fiber ring device demonstration for the Phase I feasibility study. The waveguide-based device, with compactness, high speed, and lower cost batch fabrication, is still a potential research direction for future study.

(4) We demonstrated fiber/waveguide pigtailing. This demonstration showed that current piezoelectric driven ring resonators can be replaced by fiber pigtailed waveguide phase modulators to obtain GHz crossbar reconfiguration speeds.

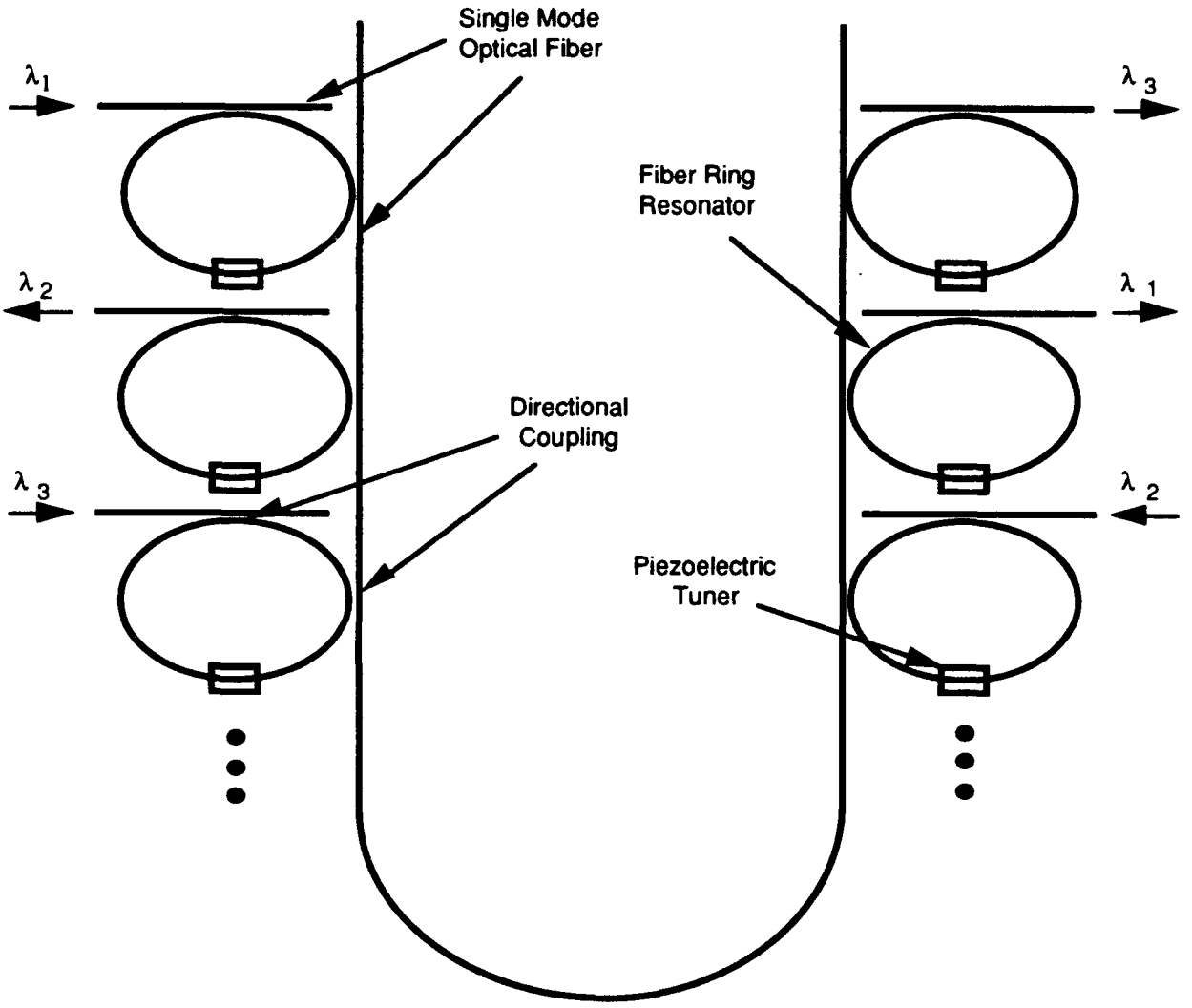

Figure 1-1
Fiber-based N x N crossbar switching system using only 2N switches.

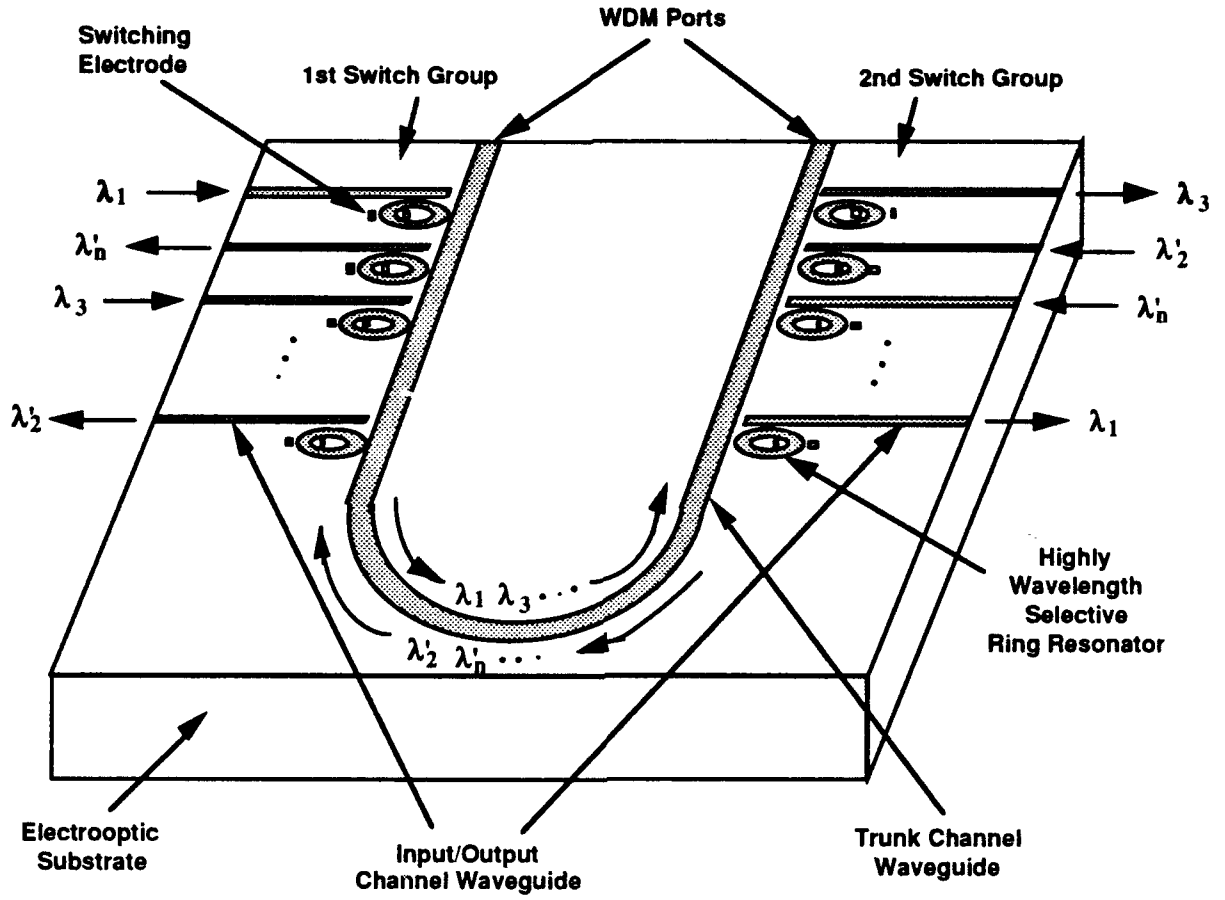

Figure 1-2
Waveguide-based N x N crossbar switching system using also only 2N switches.

2.0 THE CROSSBAR SWITCH

2.1 Switch Structure

A novel device structure for N x N crossbar switching, using only 2N switching elements is depicted in Figures 1-1 and 1-2. This device, as proposed by POC, is suitable for multi-wavelength applications with recently demonstrated wavelength selectable laser light sources [5] or multiple laser sources. Electro-optic tunable ring resonators are the fundamental switching elements that perform the required wavelength selective switching, fan-in, and fanout. Wavelength selectivity comes from the ring mode condition. Only the incoming wavelengths that satisfy the ring mode condition can be resonantly coupled and transmitted from the input channel to the trunk fiber (or waveguide), and visa versa. Any incoming signal wavelength, say λ_3, can be fed into the trunk fiber (or waveguide) after tuning the switching voltage on electrode #3 of the first switch

group so that the ring resonant condition on ring #3 is satisfied. The signal propagating on $\lambda 3$ in the trunk fiber (or waveguide) can be selectively picked up by any of the switching elements of the second switch group by similarly tuning the ring resonance. Using this type of crossbar structure, any two-way non-blocking switching pattern can be realized with a minimum number (2N) of electro-optic switching elements. This includes one-to-many fan-outs, many-to-one fan-ins, and many-to-many data communication patterns. Active wavelength division multiplexing and demultiplexing can also be performed with crossbar switch system.

To perfect the novel N x N crossbar as a fundamental building block, the tunable ring resonator switch schematically depicted in Figure 2-1 for the fiber device or Figure 2-2 for the waveguide device must first be studied and understood. Our Phase I research objective was to perform a feasibility analysis for the N x N crossbar switch. Thus, demonstrating suitable ring resonator switch performance, for either the fiber-ring or the waveguide ring, was the primary concern. During device design and fabrication, we considered the effects of mode effective index, the coupling constant from the straight channel to the ring, propagation loss, bending loss, ring size, tuning performance, switch throughput, and multi-wavelength crosstalk.

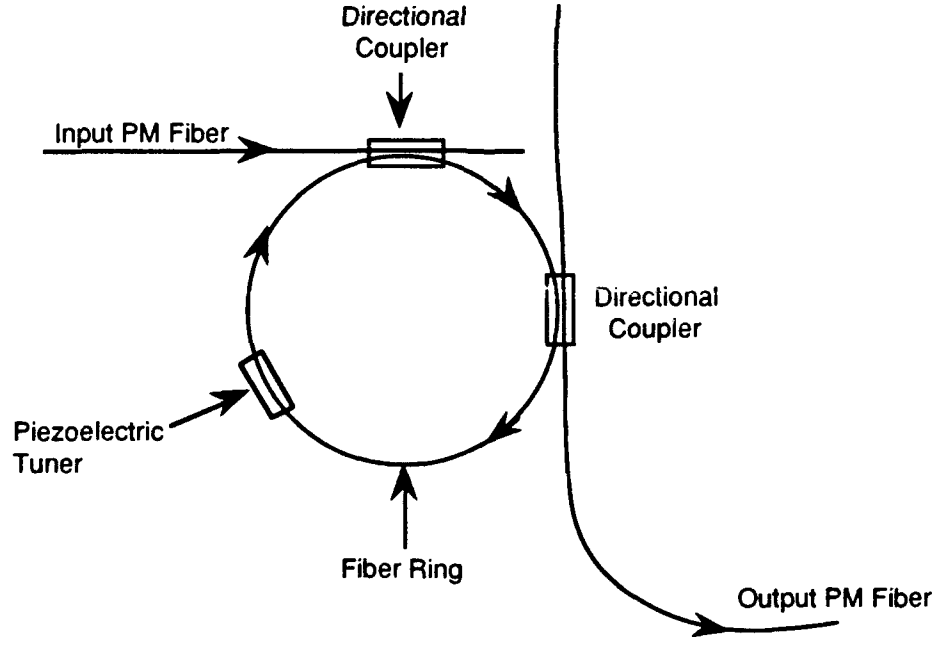

Figure 2-1
Fiber ring switch element.

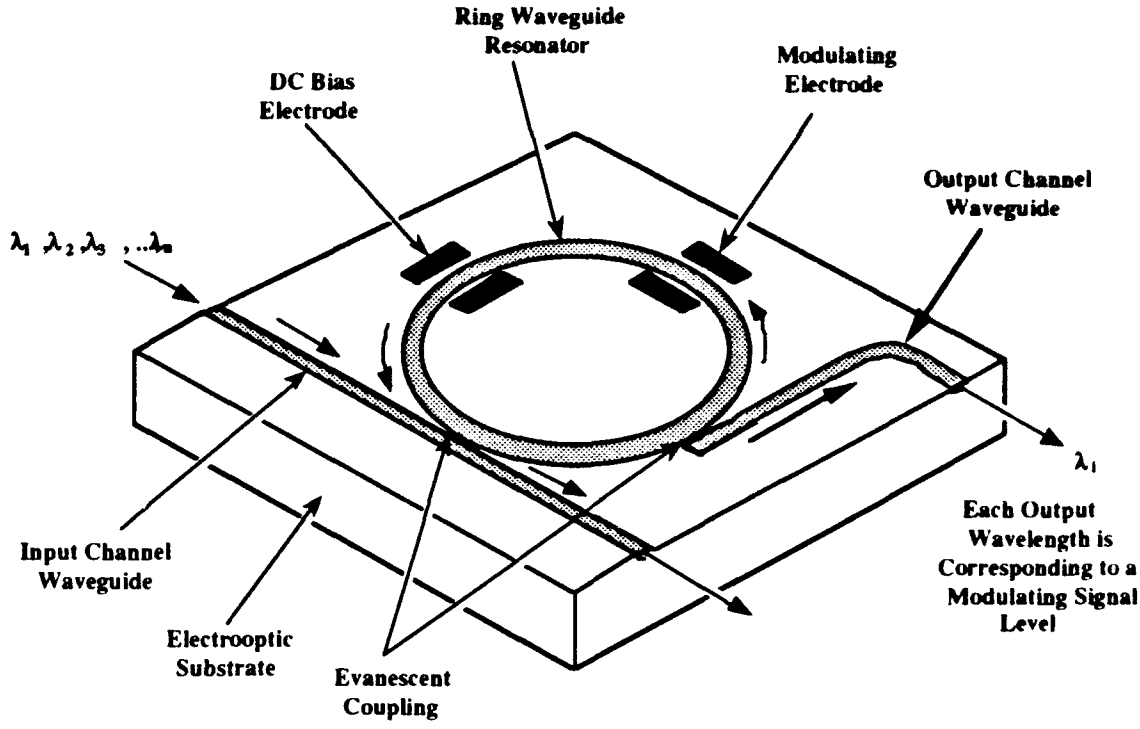

Figure 2-2
Waveguide ring switch element.

2.2 Ring Resonator

The ring resonator [6] is a loop in which light is made to interfere with itself. If the dimensions of the resonator are fixed, particular wavelengths will constructively interfere and produce a high coupling intensity in the ring while others will have destructive interference and cause negligible coupling from the straight channel and the ring. For the sake of generality, in this section, the theoretical modeling applies to both fiber and waveguide ring devices.

Consider the ring resonator depicted in Figure 2-3. This type of ring resonator is a direct coupled ring resonator [7]. The input directional coupler has a power coupling ratio, k_1, and excess loss, g_1, while the output directional coupler (or tap coupler) has a power coupling ratio, k_2, and excess loss, g_2. The ring length from the input coupler to the output coupler is ℓ_1 and the ring length from the output coupler to the input coupler is ℓ_2. The input optical field components to the couplers are designated with a superscript t and the output optical field components from the couplers are designated with a superscript a.

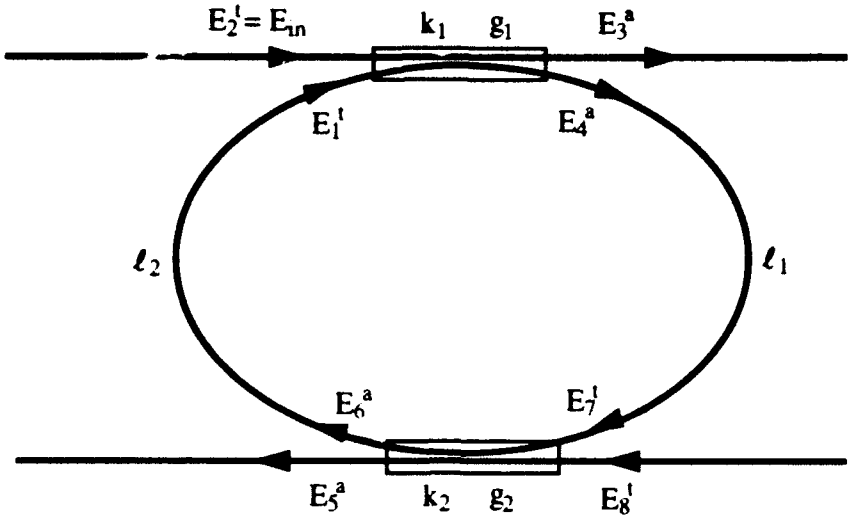

Figure 2-3
Direct coupled ring resonator couplings and field definitions.

The relationship between the field components are:

$$E_1^t = E_6^a \exp[(-\alpha + j\beta)\,\ell_2] \tag{1}$$

$$E_2^t = E_{in} \tag{2}$$

$$E_7^t = E_4^a \exp[(-\alpha + j\beta)\,\ell_1] \tag{3}$$

$$E_3^a = (1-k_1)^{1/2}\,(1-g_1)^{1/2}\,E_2^t + j\,k_1^{1/2}\,(1-g_1)^{1/2}\,E_1^t \tag{4}$$

$$E_4^a = (1-k_1)^{1/2}\,(1-g_1)^{1/2}\,E_1t + j\,k_1^{1/2}\,(1-g_1)^{1/2}\,E_2^t \tag{5}$$

$$E_5^a = (1-k_2)^{1/2}\,(1-g_2)^{1/2}\,E_8t + j\,k_2^{1/2}\,(1-g_2)^{1/2}\,E_7^t \tag{6}$$

$$E_6^a = (1-k_2)^{1/2}\,(1-g_2)^{1/2}\,E_7t + j\,k_2^{1/2}\,(1-g_2)^{1/2}\,E_8^t \tag{7}$$

where α is the field attenuation constant in the ring and β is the propagation constant of the optical mode. There is no input from port 8 and all power circulation is in a clockwise direction. Thus, we have $E_8^t = 0$. The solution of these equations is:

$$\frac{E_5^a}{E_{in}} = \frac{-(1-g_1)^{1/2}(1-g_2)^{1/2}k_1^{1/2}k_2^{1/2}\exp[(-\alpha+j\beta)\ell_1]}{1-(1-k_1)^{1/2}(1-g_1)^{1/2}(1-k_2)^{1/2}(1-g_2)^{1/2}\exp[-\alpha(\ell_1+\ell_2)+j\beta(\ell_1+\ell_2)]} \tag{8}$$

The transmission coefficient T, from input port 2 to output port 5, is given by

$$T = \left|\frac{E_5^a}{E_{in}}\right|^2 = \frac{T_1\ T_2\exp(-2\alpha\ell_1)}{(1-\sqrt{X_1}\ X_2)^2 + 4\sqrt{X_1}\ X_2\sin^2\left(\frac{\beta(\ell_1+\ell_2)}{2}\right)} \tag{9}$$

where

$$T_1 = k_1\,(1\text{-}g_1) \tag{10}$$

$$T_2 = k_2\,(1\text{-}g_2) \tag{11}$$

$$X_1 = (1\text{-}k_1)\,(1\text{-}g_1)\exp(-2\alpha\,\ell_1) \tag{12}$$

$$X_2 = (1\text{-}k_2)\,(1\text{-}g_2)\exp(-2\alpha\,\ell_2) \tag{13}$$

The maximum transmission, T_{max}, and minimum transmission, T_{min}, can be expressed as

$$T_{max} = \frac{T_1\ T_2\exp(-2\alpha\ell_1)}{(1-\sqrt{X_1}\ X_2)^2} \tag{14}$$

$$T_{min} = \frac{T_1\ T_2\exp(-2\alpha\ell_1)}{(1+\sqrt{X_1}\ X_2)^2} \tag{15}$$

respectively. A simple derivation gives the finesse, F, of the ring resonator to be

$$F = \frac{\pi\,(X_1X_2)^{1/4}}{1-\sqrt{X_1X_2}} \tag{16}$$

The free spectral range, FSR, and free wavelength range, FWR, are given by

$$FSR = \frac{c}{n(\ell_1 + \ell_2)} \tag{17}$$

$$FWR = \frac{\lambda^2}{n(\ell_1 + \ell_2) - \lambda} \tag{18}$$

while the corresponding frequency and wavelength transmission bandwidth (FWHM) can be expressed as

$$\Delta f = \frac{FSR}{F} \tag{19}$$

$$\Delta\lambda = \frac{FWR}{F} \tag{20}$$

These equations are general and can be applied to any ring type resonator provided that the specified device parameters are known. Hence, they can be used to analyze fiber ring resonators as well as waveguide ring resonators.

When a cross coupled ring resonator [8] is used, see Figure 2-4, the formulas are slightly different.

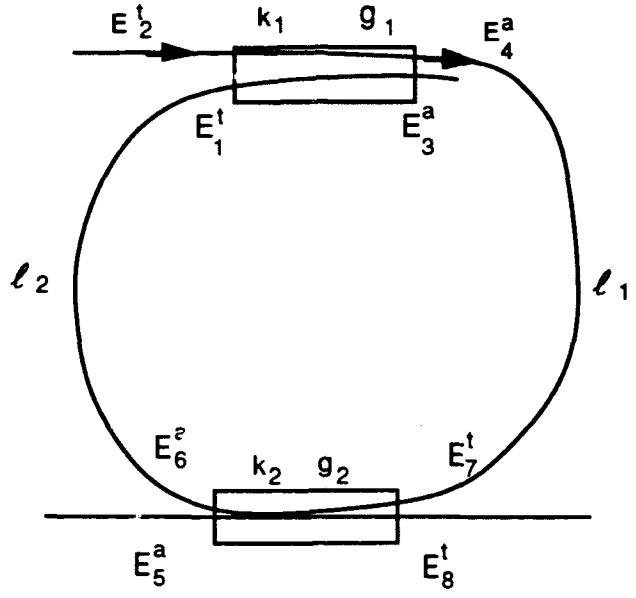

Figure 2-4
Cross coupled ring resonator couplings and field definitions.

With field components defined in Figure 2-4, their relationships are:

$$E_1^t = E_6^a \exp[(-\alpha + j\beta)\,\ell 2] \tag{21}$$

$$E_2^t = E_{in} \tag{22}$$

$$E_7^t = E_4^a \exp[(-\alpha + j\beta)\,\ell_1] \tag{23}$$

$$E_3^a = (1-k_1)^{1/2}\,(1-g_1)^{1/2}\,E_1^t + j\,k_1^{1/2}(1-g_1)^{1/2}\,E_2^t \tag{24}$$

$$E_4^a = (1-k_1)^{1/2}\,(1-g_1)^{1/2}\,E_2t + j\,k_1^{1/2}\,(1-g_1)^{1/2}\,E_1^t \tag{25}$$

$$E_5^a = (1-k_2)^{1/2}\,(1-g_2)^{1/2}\,E_8^t + j\,k_2^{1/2}\,(1-g_2)^{1/2}\,E_7^t \tag{26}$$

$$E_6^a = (1-k_2)^{1/2}\,(1-g_2)^{1/2}\,E_7^t + j\,k_2^{1/2}\,(1-g_2)^{1/2}\,E_8^t \tag{27}$$

Obviously, only Eqs. (24) and (25) are different than Eqs. (4) and (5) for the direct coupled ring resonator. Similar derivation results in the transmission coefficient

$$T = \left|\frac{E_s a}{E_{in}}\right|^2_2 = \frac{b\ \exp(-2\alpha \ell_1)}{1 + 2\ a\ \exp\left(-\alpha(\ell_1 + \ell_2)\right) \sin\beta\ (\ell_1 + \ell_2) + a^2 \exp\left(-2\ \alpha(\ell_1 + \ell_2)\right)} \quad (28)$$

where

$$a = \sqrt{k_1 (1 - g_1)(1 - k_2)(1 - g_2)} \quad (29)$$

$$b = k_2 (1 - g_2)(1 - k_1)(1 - g_1) \quad (30)$$

The maximum and minimum transmission, in this case, can be expressed as

$$T_{max} = \frac{b\ \exp(-2\alpha \ell_1)}{\left[1 - a\ \exp\left(-\alpha\ (\ell_1 + \ell_2)\right)\right]^2} \quad (31)$$

$$T_{min} = \frac{b\ \exp(-2\alpha \ell_1)}{\left[1 + a\ \exp\left(-\alpha\ (\ell_1 + \ell_2)\right)\right]^2} \quad (32)$$

The finesse of the cross coupled ring resonator is

$$F = \frac{\pi \sqrt{a\ \exp\left(-\alpha(\ell_1 + \ell_2)\right)}}{\left[1 - a\ \exp\left(-\alpha\ (\ell_1 + \ell_2)\right)\right]} \quad (33)$$

The equations for free spectral range, free wavelength range, and selectivity bandwidths are identical to the direct coupled ring resonator (Eqs. (17) to (20)).

2.3 Resonance Tuning

For either direct coupled or cross coupled ring resonator, the resonance coupling mode condition is given as

$$m\lambda = n\ell + \Delta n_{DC} L_{DC} + \Delta n L \qquad (34)$$

where m is the resonator mode number assuming integer values, λ is the free space wavelength, n is the effective index of the ring fiber or waveguide, Δn is the index modulation tuned by the electro-optic effect or piezoelectric effect, ℓ is the resonator loop length, L is the electrode length, and Δn_{DC} is the index modulation set by the DC bias for initial adjustment by a DC electrode with length L_{DC} (see Figure 2-2). The effective use of DC bias sets the threshold voltage and compensates for thermal effects.

For a set values of n, ℓ, Δn_{DC}, L_{DC}, Δn, and L, the wavelength λ that satisfies Eq. (34) with an integer m will give resonant coupling. However, a wavelength shifting away from this coupling condition will not satisfy the equation, resulting in a low coupling intensity until another integer $m \pm 1$ is reached. Figure 2-5 shows a spectral response of the resonator at ports 3 and 5 of Figures 2-3 and 2-4. The spectral frequency of an optical wave is related to its wavelength by $f = c/\lambda$, where c is the light speed in vacuum. The width of the resonance, Δf, is defined as the full width at half maximum and can be calculated with Eq. (19). The free spectral range calculated with Eq. (17) is also defined as the frequency separation between the two response peaks. The output waveform at port 5 is inverted from that of port 3, because of the resonant coupled energy loss and gain at these ports. When at resonance, the light in the loop resonator actually interferes destructively (in direct coupled ring resonators) or constructively (in cross coupled ring resonators) with the light in the feeder channel. Energy accumulates in the ring and the output port 5 has a high-intensity. When at off resonance, less energy will be coupled into the ring so that port 3 has a high-intensity throughput but port 5 receives less optical power.

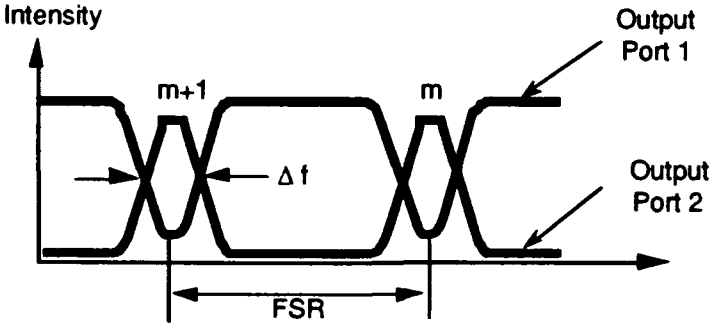

Figure 2-5
The output of ring resonator as a function of input optical frequency.

The transmission performance at port 5 is similar to a two-mirror Fabry-Perot resonator system. However, in contrast to two-mirror Fabry-Perot resonators, the ring resonator suppresses unwanted back reflection that causes instability in the wavelength and intensity of the laser diode sources. Secondly, ring resonators allow the wavelength multiplexing and demultiplexing (see Figures 1-1 and 1-2) that two-mirror Fabry-Perot devices cannot perform alone. The finesse of the ring resonator system is equal to the FSR divided by Δf and can be found with Eq. (16) or (33). The larger the finesse, the better the wavelength selectivity with a fixed loop length.

2.4 Calculation Results

Based on the above ring resonator formulations, we analyzed the effect of coupler efficiencies, losses, and ring loop lengths to the selectivity and system throughput.

Tables 1 to 3 show computer-calculated results of various coupling efficiencies for direct coupled fiber ring resonators. As can be seen, weak coupling (2%) at both input and output couplers result in a strong resonance with a finesse of more than 100 and maximum transmission of 44.13%. Increasing the coupler's coupling efficiency to 3% decreases the finesse to 77.5, but increases the maximum transmission to over 55%. In both cases, we assumed a coupler excess loss of 1%. Reducing the coupler loss can significantly improve the finesse value. For a resonator with weak input coupling and no tap coupling, the finesse can be even higher. Table 3 shows less than 0.5% input coupling and 0.1% coupler loss. The finesse in this case can be over 1000. In fact, experimental results obtained by others [9] have confirmed the possibility of such extremely high finesse. In our crossbar structure, tap or output couplers are required. Thus, a reasonable expectation for finesse is on the order of 50 to 100. When the finesse is 100, it is possible to construct a 100 x 100 crossbar switch that may never be possible based on other crossbar architectures. Resonant tuning can be performed using either a piezoelectric technique or a thermal-control technique for the fiber-based ring device. Resonant tuning can also be performed by using low-loss fiber-pigtailed waveguide phase modulator, as will be discussed later, for high speed reconfiguration advantages.

Table 1 Fiber-Based Ring Resonator with 2% Input and Output Couplings

Ring Resonator Calculation Results	
Input Coupler Efficiency =	.02000
Input Coupler Loss =	.01000
Tap Coupler Efficiency =	.02000
Tap Coupler Loss =	.01000
Input To Tap Coupler Distance =	100.00000 mm
Tap To Input Coupler Distance =	100.00000 mm
Laser Wavelength =	632.80000 nm
Ring Propagation Loss =	- .200 dB/km
Refractive Index Of The Ring =	1.45670
Total Transmission =	.02733 %
Finesse =	103.82409
Maximum Transmission =	44.13322 %
Minimum Transmission =	.01010 %
Free Spectral Range =	1029.012483 MHz
Frequency Bandwidth (FWHM) =	9.911115 MHz
Free Wavelength Range =	.0013745 nm
Wavelength Bandwidth (FWHM) =	.0000132 nm

Table 2 Fiber-Based Ring Resonator with 3% Input and Output Couplings

Ring Resonator Calculation Results	
Input Coupler Efficiency =	.03000
Input Coupler Loss =	.01000
Tap Coupler Efficiency =	.03000
Tap Coupler Loss =	.01000
Input To Tap Coupler Distance =	100.00000 mm
Tap To Input Coupler Distance =	100.00000 mm
Laser Wavelength =	632.80000 nm
Ring Propagation Loss =	- .200 dB/km
Refractive Index Of The Ring =	1.45670
Total Transmission =	.06209 %
Finesse =	77.53779
Maximum Transmission =	55.95426 %
Minimum Transmission =	.02295 %
Free Spectral Range =	1029.012483 MHz
Frequency Bandwidth (FWHM) =	13.271109 MHz
Free Wavelength Range =	.0013745 nm
Wavelength Bandwidth (FWHM) =	.0000177 nm

Table 3 Fiber-Based Ring Resonator with 0.5% Input Coupling and No Output Coupling

Ring Resonator Calculation Results	
Input Coupler Efficiency =	.00500
Input Coupler Loss =	.00100
Tap Coupler Efficiency =	.00000
Tap Coupler Loss =	.00000
Input To Tap Coupler Distance =	100.00000 mm
Tap To Input Coupler Distance =	100.00000 mm
Laser Wavelength =	632.80000 nm
Ring Propagation Loss =	- .200 dB/km
Refractive Index Of The Ring =	1.45670
Total Transmission =	.00000 %
Finesse =	1043.32766
Maximum Transmission =	.00000 %
Minimum Transmission =	.00000 %
Free Spectral Range =	1029.012483 MHz
Frequency Bandwidth (FWHM) =	.986279 MHz
Free Wavelength Range =	.0013745 nm
Wavelength Bandwidth (FWHM) =	.0000013 nm

Tables 4 to 7 show the effect of reducing the loop length. For a low-loss fiber-based ring resonator, reducing the loop length from 300 mm (150 mm + 150 mm) to 100 mm increases the finesse from 103.816 to 103.832 while the maximum transmission under a proper tuning bias changes from 44.13% to 44.14% (Tables 4 and 5). Clearly, for a low-loss ring, the effect to the maximum transmission and finesse is negligible. However, the free spectral range increases from 666.21 MHz to 1998.62 MHz and the frequency selectivity bandwidth increases from 6.42 MHz to 19.25 MHz. We found that when the laser linewidth is not very narrow (see Section 2.6), it is desirable to use a ring resonator with small loop length and large frequency selectivity bandwidth. Furthermore, a small loop length allows faster device response, especially useful for high data rate applications. The waveguide-based ring resonator may be more desirable than the fiber-based resonator with a small loop length due to batch fabrication advantages.

Table 4 Fiber-Based Ring Resonator with 300-mm Loop Length

Ring Resonator Calculation Results	
Input Coupler Efficiency =	.02000
Input Coupler Loss =	.01000
Tap Coupler Efficiency =	.02000
Tap Coupler Loss =	.01000
Input To Tap Coupler Distance =	150.00000 mm
Tap To Input Coupler Distance =	150.00000 mm
Laser Wavelength =	632.80000 nm
Ring Propagation Loss =	- .200 dB/km
Refractive Index Of The Ring =	1.50000
Total Transmission =	.07009 %
Finesse =	103.81618
Maximum Transmission =	44.12651 %
Minimum Transmission =	.01010 %
Free Spectral Range =	666.205549 MHz
Frequency Bandwidth (FWHM) =	6.417165 MHz
Free Wavelength Range =	.0008899 nm
Wavelength Bandwidth (FWHM) =	.0000086 nm

Table 5 Fiber Ring Resonator with 100-mm Loop Length

Ring Resonator Calculation Results	
Input Coupler Efficiency =	.02000
Input Coupler Loss =	.01000
Tap Coupler Efficiency =	.02000
Tap Coupler Loss =	.01000
Input To Tap Coupler Distance =	50.00000 mm
Tap To Input Coupler Distance =	50.00000 mm
Laser Wavelength =	632.80000 nm
Ring Propagation Loss =	- .200 dB/km
Refractive Index Of The Ring =	1.50000
Total Transmission =	.01601 %
Finesse =	103.83199
Maximum Transmission =	44.13994 %
Minimum Transmission =	.01010 %
Free Spectral Range =	1998.616646 MHz
Frequency Bandwidth (FWHM) =	19.248564 MHz
Free Wavelength Range =	.0026696 nm
Wavelength Bandwidth (FWHM) =	.0000257 nm

Tables 6 and 7 show the effect of reducing the loop length under a relatively high loop propagation loss. The present loop propagation of -0.2 dB/cm or -20000 dB/km is suitable to describe a conventional optical waveguide. Changing the loop length from 100 mm (50 mm + 50 mm) to 20 mm increases the free spectral range from 1998.62 MHz to 9993.08 MHz and the frequency bandwidth from 166.20 MHz to 242.78 MHz. This effect is the same predicted in the low loop loss case. However in this case, the maximum transmission increases from 0.59% to 6.94% while the finesse increases from 12.03 to 41.16. The small increase in maximum transmission can be compensated for by using other coupling efficiency values with some trade-off in system finesse.

Table 6 Lossy Ring Resonator (-0.2 dB/cm) with 100-mm Loop Length

Ring Resonator Calculation Results	
Input Coupler Efficiency =	.02000
Input Coupler Loss =	.01000
Tap Coupler Efficiency =	.02000
Tap Coupler Loss =	.01000
Input To Tap Coupler Distance =	50.00000 mm
Tap To Input Coupler Distance =	50.00000 mm
Laser Wavelength =	632.80000 nm
Ring Propagation Loss =	-20000.000 dB/km
Refractive Index Of The Ring =	1.50000
Total Transmission =	.01560 %
Finesse =	12.02529
Maximum Transmission =	.59205 %
Minimum Transmission =	.00993 %
Free Spectral Range =	1998.616646 MHz
Frequency Bandwidth (FWHM) =	166.201149 MHz
Free Wavelength Range =	.0026696 nm
Wavelength Bandwidth (FWHM) =	.0002220 nm

Table 7 Lossy Ring Resonator (-0.2 dB/cm) with-20 mm Loop Length

Ring Resonator Calculation Results		
Input Coupler Efficiency =	.02000	
Input Coupler Loss =	.01000	
Tap Coupler Efficiency =	.02000	
Tap Coupler Loss =	.01000	
Input To Tap Coupler Distance =	10.00000	mm
Tap To Input Coupler Distance =	10.00000	mm
Laser Wavelength =	632.80000	nm
Ring Propagation Loss =	-20000.000	dB/km
Refractive Index Of The Ring =	1.50000	
Total Transmission =	.01306	%
Finesse =	41.16167	
Maximum Transmission =	6.93674	%
Minimum Transmission =	.01009	%
Free Spectral Range =	9993.083228	MHz
Frequency Bandwidth (FWHM) =	242.776448	MHz
Free Wavelength Range =	.0133481	nm
Wavelength Bandwidth (FWHM) =	.0003243	nm

2.5 Phase I Prototype Structure Selection and Design

Waveguide-based ring resonators use channel waveguide structures instead of low-loss optical fibers. The advantages of the waveguide structure are its compact structure, capability of being batch fabricated, and its high-speed electro-optic tunability. However, the waveguide devices suffer from large waveguide propagation loss. Low-loss waveguides (-2.6 dB/m or - 0.026 dB/cm) have been demonstrated on silica-on-silicon waveguides [10]. Based on this technology, a wide FSR waveguide double-ring resonator with a firesse of 182 has been demonstrated [6]. This silica-on-silicon waveguide technology does not take advantage of high-speed electro-optic tuning. Rather, it relies on thermal optic tuning with a typical speed of less than 0.8 msec.

On an electro-optic substrate, waveguides generally have higher loss; in a proton exchanged Z-cut $LiNbO_3$ waveguide, the loss is on the order of -0.2 dB/cm--about one order of magnitude higher than the silica-on-silicon waveguide. The higher loss greatly reduces the finesse and maximum transmission of the ring resonator. Results, based on a loss of -0.2 dB/cm or -20000 dB/km, are given in Tables 8 and 9. A smaller ring size, $\ell_1 = \ell_2 = 10$ mm, was used in these calculations because of the integrated structure. Both weak and strong coupling cases are shown. Under 2%

weak coupling and 1% coupler loss, the device will have a finesse of about 41 and only 6.9% maximum transmission. Compared to fiber devices, the waveguide loss has a strong effect on finesse and maximum transmission. With 10% coupling and 1% coupler loss, the device will have a better maximum transmission of 42% but a poorer finesse, only 19.4. Clearly, there is a trade-off between resonator finesse and maximum throughput transmission.

These calculations have assumed that there is no additional waveguide loss due to bending. In fact, a small bending radius will produce additional bending loss in the waveguide. Based on theoretical estimations [11] for a ring size of $\ell_1 = \ell_2 = 10$ mm, the bending loss is generally negligible. However, the experimental results are much poorer than the theoretical predictions. For a 1-cm-diameter ring waveguide on a proton exchanged Z-cut $LiNbO_3$ waveguide, the total ring loss has been measured at about -4.5 dB [12]. After subtracting the propagation loss of -0.2 dB/cm, the bending loss alone, for the ring of length $\ell_1 + \ell_2 = 31.4$ mm, is -3.872 dB. The bending loss dominates the other ring waveguide loss.

The large bending loss may result from scattering at the relatively rough curved waveguide boundary due to imperfect fabrication. This technological difficulty is yet to be overcome. Thus, the demonstration of such waveguide-based ring device requires extra support. Recent experiments under such high-loss conditions have been performed at the University of Florida [12] under the sponsorship of Harris Corporation. The ring resonator used in the experiments is depicted in Figure 2-6. It consists of only a single input coupler with a measured 25% coupling efficiency. The coupler length is 2 mm with a 5.5 mm coupler gap. The channel waveguide width is 4.5 mm and the wavelength used for the measurement is 1.3 μm. The device is fabricated under proton exchange at 220°C and is partially annealed under 360°C for 2 hr. Their final device has a device length of about 18 mm. The measured finesse is about 8.

Table 8 Waveguide-Based Ring Resonator with 2% Couplings and -0.2 dB/cm Propagation Loss

Ring Resonator Calculation Results	
Input Coupler Efficiency =	.02000
Input Coupler Loss =	.01000
Tap Coupler Efficiency =	.02000
Tap Coupler Loss =	.01000
Input To Tap Coupler Distance =	0.00000 mm
Tap To Input Coupler Distance =	0.00000 mm
Laser Wavelength =	632.80000 nm
Ring Propagation Loss =	-20000.000 dB/km
Refractive Index Of The Ring =	2.20/00
Total Transmission =	.04320 %
Finesse =	41.16167
Maximum Transmission =	6.93674 %
Minimum Transmission =	.01009 %
Free Spectral Range =	6810.370214 MHz
Frequency Bandwidth (FWHM) =	165.454190 MHz
Free Wavelength Range =	.0090968 nm
Wavelength Bandwidth (FWHM) =	.0002210 nm

Table 9 Waveguide-Based Ring Resonator with 10% Couplings and -0.2 dB/cm Propagation Loss

Ring Resonator Calculation Results	
Input Coupler Efficiency =	.10000
Input Coupler Loss =	.01000
Tap Coupler Efficiency =	.10000
Tap Coupler Loss =	.01000
Input To Tap Coupler Distance =	10.00000 mm
Tap To Input Coupler Distance =	10.00000 mm
Laser Wavelength =	632.80000 nm
Ring Propagation Loss =	-20000.000 dB/km
Refractive Index Of The Ring =	2.20100
Total Transmission =	1.15110 %
Finesse =	19.43598
Maximum Transmission =	42.10229 %
Minimum Transmission =	.27322 %
Free Spectral Range =	6810.370214 MHz
Frequency Bandwidth (FWHM) =	350.400194 MHz
Free Wavelength Range =	.0090968 nm
Wavelength Bandwidth (FWHM) =	.0004680 nm

Clearly, the high loss and low finesse of the experimental results for the waveguide ring are not encouraging. We may repeat a similar experiment in Phase I with more care in hopes of achieving a better result. However, the chance of success is minimal because, in our device structure, an output coupler must be added, which will increase the total ring loss and further reduce the device finesse. Therefore, this waveguide-based ring for the N x N crossbar was too risky and unrealistic for the scope of Phase I. Since the major effort in Phase I has been to demonstrate the feasibility of the ring resonators based crossbar, a better approach, utilizing maturely developed fiber-based ring resonators, was proposed and approved by the program monitor. This approach can in fact reduce the time required to commercialize the proposed N x N crossbar switch design.

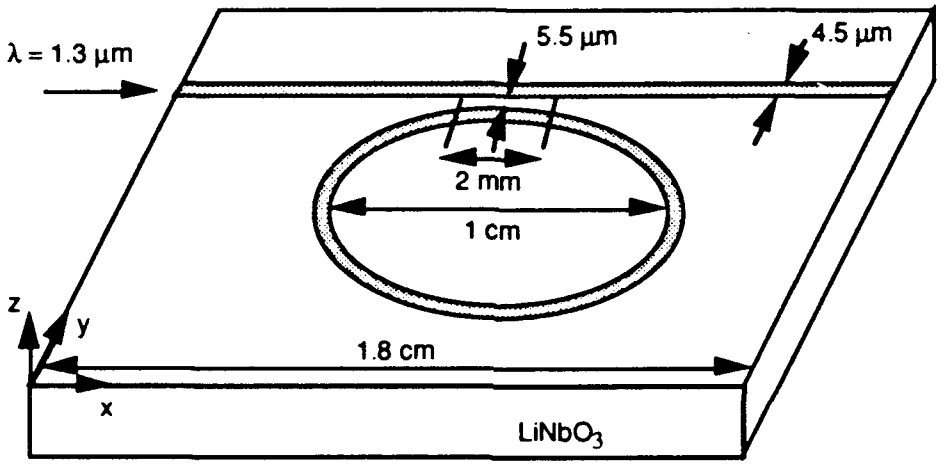

Figure 2-7
Waveguide-based ring resonator developed at the University of Florida.

The original motivation for using a waveguide-based ring resonator for the N x N crossbar was to take advantage of the high-speed tuning potential of integrated electro-optic devices. We can still achieve the high-speed tuning performance without using a waveguide-based ring if we consider a modified device structure, as shown in Figure 2-8, which is similar to the device shown in Figure 1-1 but with electro-optic phase modulators instead of the piezoelectric tuners. A high-performance fiber optic ring resonator is used. Tuning is achieved by using a fiber pigtailed single-mode waveguide phase modulator. The total ring loss in this case will be dominated by the fiber/waveguide pigtailing loss since the fiber by itself is extremely low loss. Fiber pigtailed single-mode waveguide phase modulators are now commercially available from Crystal Technology, Inc. and from United Technologies Photonics. The phase modulator can operate at a speed of a few GHz. The commercial fiber-waveguide-fiber pigtailing loss is on the order of -3 to

-4 dB. Reducing pigtailing loss is in fact an engineering issue. Low loss pigtailing of nearly -1 dB has already been demonstrated at Litton Guidance and Control Systems. Therefore, we considered a modified approach using a fiber-based ring and waveguide modulator the more realistic near-term approach. To do so, in Phase I, we demonstrated:

1. a fiber-based ring resonator with piezoelectric tuning capability. This demonstration will show the feasibility of the novel N x N crossbar switch to operate at low speed,

2. fiber/waveguide pigtailing at POC facilities.

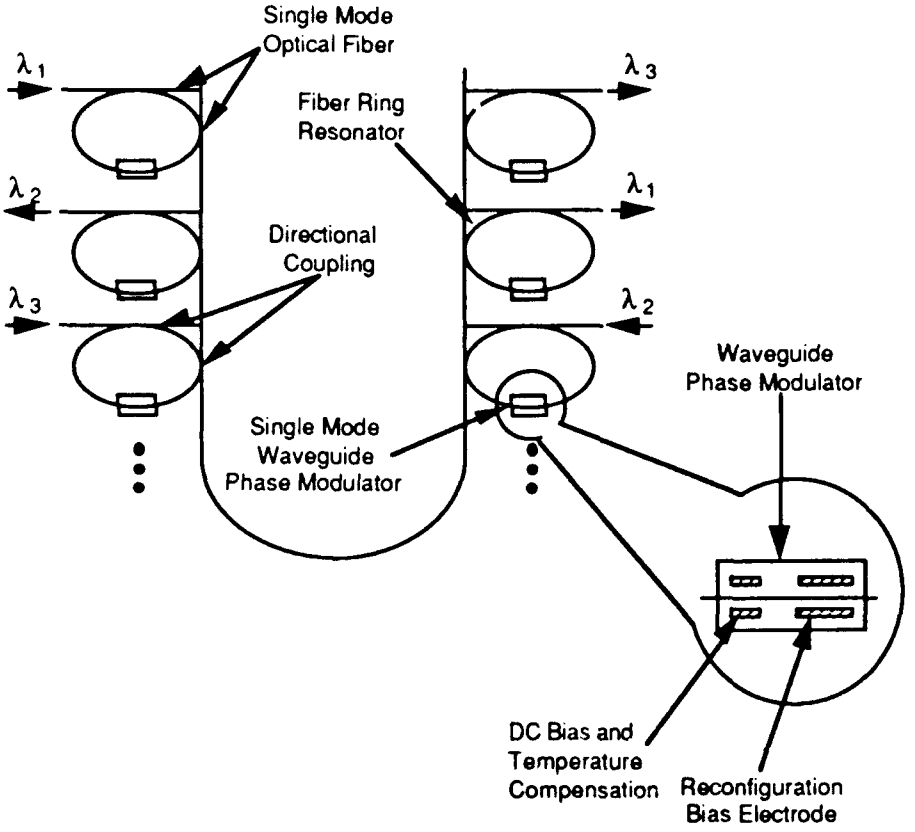

Figure 2-8
Modified N x N crossbar switch structure using pigtailed waveguide electro-optic phase modulators.

There are two types of fiber-based ring resonators: direct coupled and cross coupled. The difference between the two types is in the fiber wiring mechanism, as described in Section 2.2. In a direct coupled fiber-based ring resonator, there must be a splice in the ring since the fiber does not originally come with a ring. The splice loss will degrade the performance of the ring resonance. Therefore, the best choice for the fiber-based ring resonator is the cross coupled structure where there is no splice in the ring.

The transmission response of the cross coupled ring resonator differs from the direct coupled ring resonator by only a phase or bias difference. However, to produce the same transmission peak at the same output (tap) coupler efficiency and loss, the input coupling efficiencies must be complementary to each other. In other words, if the input coupler efficiency is 3% for a direct coupled ring, to produce the same transmission response except for phase or bias, the input coupler efficiency for the cross coupled ring device must be 97%. Figures 2-9 and 2-10 show the comparison of the two resonator responses. The computation parameters are summarized in Tables 2 and 10, respectively. The phase or bias difference can be easily compensated through the piezoelectric driven circuit.

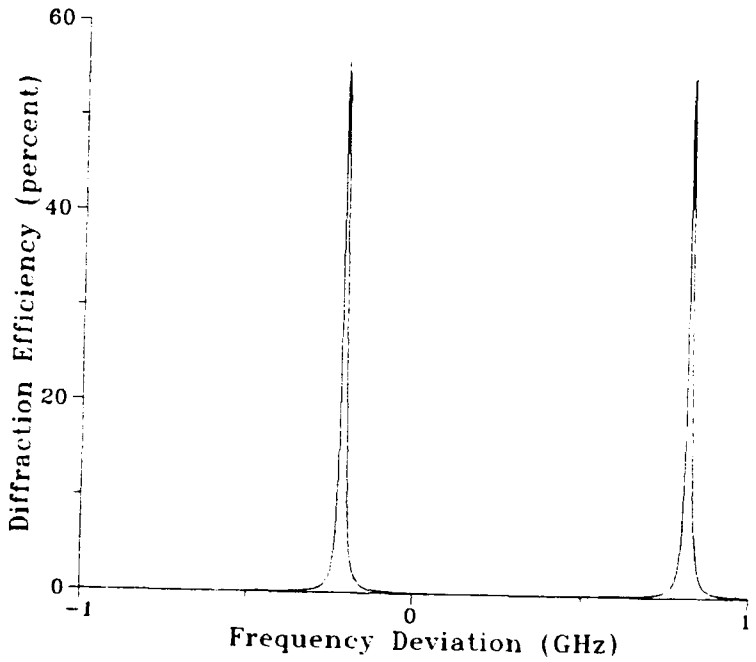

Figure 2-9
Transmission response of a direct coupled ring resonator. The device parameters and calculation results are summarized in Table 1. In the plot, the frequency deviation is calculated with respect to the center laser frequency $f = c/\lambda = 4.7376 \times 10^{14}$ Hz.

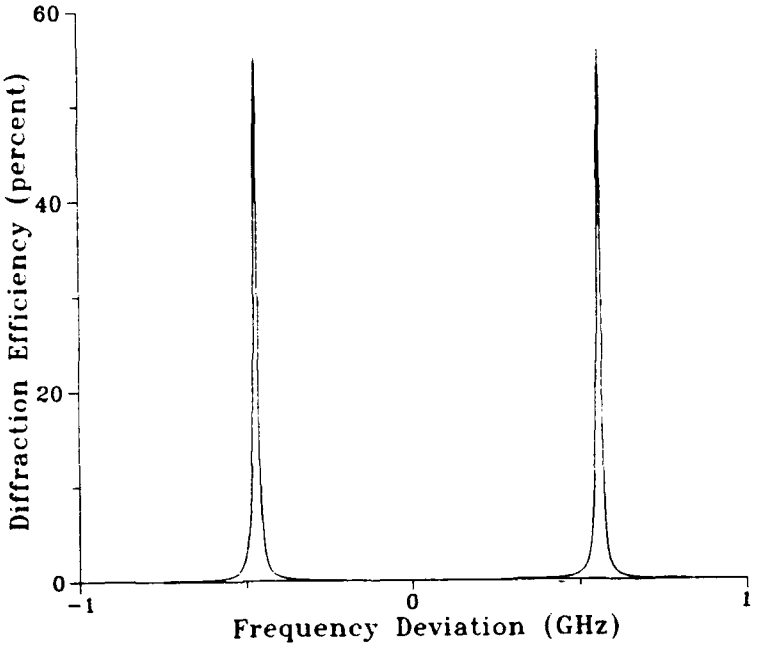

Figure 2-10
Transmission response of a cross coupled ring resonator with schematic depicted in Figure 2-4. The device parameters and calculation results are summarized in Table 10. In the plot, the frequency deviation is calculated with respect to the center laser frequency
$f = c/\lambda = 4.7376 \times 10^{14}$ Hz.

Table 10 Calculation Parameters and Results for Figure 2-10

C-Ring Resonator Calculation Results	
Input Coupler Efficiency =	.97000
Input Coupler Loss =	.01000
Tap Coupler Efficiency =	.03000
Tap Coupler Loss =	.01000
Input To Tap Coupler Distance =	100.00000 mm
Tap To Input Coupler Distance =	100.00000 mm
Laser Wavelength =	632.80000 nm
Ring Propagation Loss =	- .200 dB/km
Refractive Index Of The Ring =	1.45670
Total Transmission =	.02336 %
Finesse =	77.53779
Maximum Transmission =	55.95426 %
Minimum Transmission =	.02295 %
Free Spectral Range =	1029.012483 MHz
Frequency Bandwidth (FWHM) =	13.271109 MHz
Free Wavelength Range =	.0013745 nm
Wavelength Bandwidth (FWHM) =	.0000177 nm

2.6 Laser Linewidth Effect — An Important System Issue

The calculated wavelength selectivity bandwidth, $\Delta\lambda$, or frequency selectivity bandwidth, Δf, is based on the ideal single frequency light source. However, commercially-available light sources have finite laser linewidths. When the laser linewidth, $\Delta\lambda_L$, or Δf_L is much narrower than the $\Delta\lambda$ or Δf, the laser linewidth effect is considered negligible. When the laser linewidth is comparable to or even larger than the FWHM selectivity bandwidth, a broadening to the transmission response peak or dip will be observed. This transmission broadening effect will significantly affect the selectivity bandwidth and the finesse of the ring resonator. It will also reduce the system throughput efficiency. Ultimately, it will affect the number of crossbar channels that the ring resonator based device can support.

For example, given the fiber-based ring resonator shown in Table 2. The frequency bandwidth is 13.27 MHz while the free spectral range is 1029.01 MHz. The finesse is 77.53. Assuming a 50 MHz linewidth laser is used, the resulting frequency bandwidth is nearly 13.27 MHz + 50 MHz = 63.27 MHz. Therefore, based on definition, the finesse of the ring resonator under such laser source is

$$F = 1029.01 \text{ MHz}/63.27 \text{ MHz} = 16.26$$

The finesse drops from 77.53 to 16.26. The effect of laser linewidth is significant. Fortunately, commercially available laser diodes such as DFB lasers and gas lasers like HeNe lasers have very small laser linewidths. For example, a typical HeNe laser linewidth is on the order of 1 MHz. When it is used in the above device, the frequency bandwidth is 13.27 MHz + 1 MHz = 14.27 MHz. In this case, the system finesse is given by

$$F = 1029.01 \text{ MHz}/14.27 \text{ MHz} = 72.11$$

The ring resonator finesse decreases slightly from 77.53 to 72.11. Obviously, a narrow linewidth laser is required in the ring-resonator crossbar system. Future optical communication and computing may utilize the narrow linewidth DFB lasers (linewidth ~ 10 MHz, manufactured by Ortel Corporation, for example). When using these DFB lasers of 10 MHz linewidth, which is larger than the HeNe laser linewidth, it may be necessary to use a smaller ring size, such as 20 to 100 mm, so the finesse reduction can be small. Since these lasers already exist commercially, the fiber- or waveguide-based ring resonator based crossbar switch is suitable in the communication and computing systems.

3.0 DEVICE FABRICATION AND PERFORMANCE

3.1 Demonstration of Fiber-Based Ring Resonator Switch for Wavelength Selective Coupling and Crossbar

3.1.1 Fabrication of the Fiber-Based Ring Resonator

Since the primary goal of Phase I was to demonstrate the feasibility of the proposed ring resonator crossbar concept, we took advantage of the existing fabrication facilities of Canadian Instrumentation and Research Ltd. They fabricated our fiber-based ring resonator based on the design considerations and specifications described in the previous section.

The fabricated fiber-based ring resonator is shown in Figure 3-1. Its schematic is depicted in Figure 3-2. The resonator consists of a polarization-maintaining single-mode optical fiber, an input resonator coupler (RES), an output tap coupler (TAP), and a piezoelectric tuner. The resonator is based on the cross coupled ring resonator principle described in Section 2.2. The

input signal from port A is resonant coupled into the ring through a maximum coupling condition at RES. This maximum coupling allows a maximum ring finesse. The tap coupler was set at a relatively low coupling efficiency. The ring resonator has a ring size of approximately 23 cm and the tuning length of the piezoelectric tuner is about 3.8 cm. Both the couplers are designed and fabricated based on the fiber directional coupler principle.

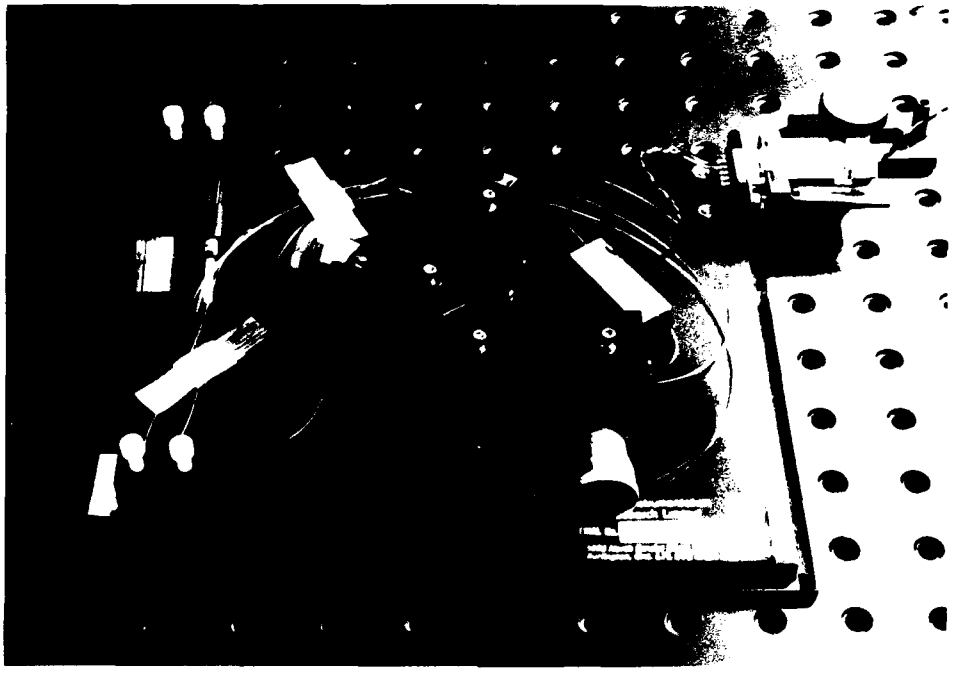

Figure 3-1
Our Phase I fiber-based ring resonator.

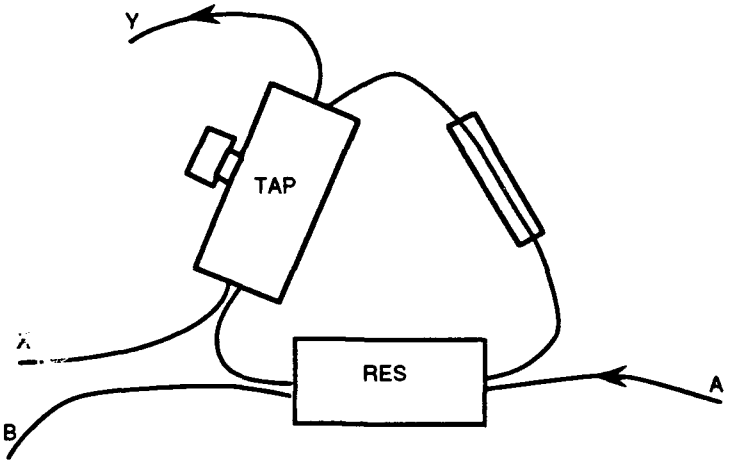

Figure 3-2
Schematic of the fiber-based ring resonator shown in Figure 3-1.

To make a fiber directional coupler, both fibers are polished into a D-shape as shown in Figure 3-3. A micrometer on the coupler was used to shift the relative transverse position of the two polished fibers (Figure 3-4). When two fibers are in adjacent positions with a minimum gap between the fiber cores, as shown in Figure 3-3, a maximum coupling is achieved by sending an optical signal from one fiber to the other through the evanescent coupling effect. Index matching oil is used in the gap of two fibers to prevent optical index discontinuity. When the two fibers are offset transversely by a reasonable amount of distance, there is no coupling between them (see Figure 3-3). Further offset of the two fiber positions will result in coupling loss through substrate radiation. Fine adjustment of the coupling condition is achieved through the lever system shown in Figure 3-4.

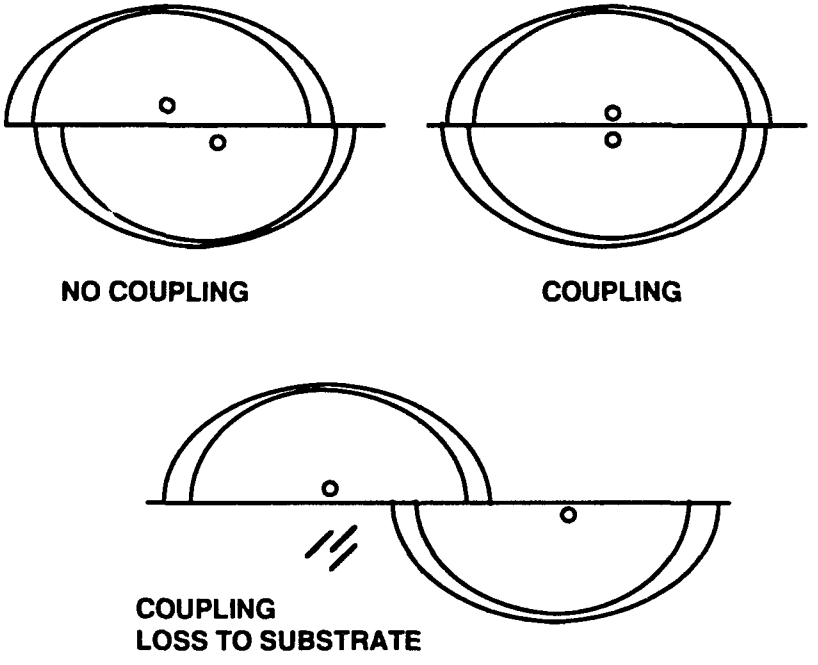

Figure 3-3
The concept of fiber directional coupler.

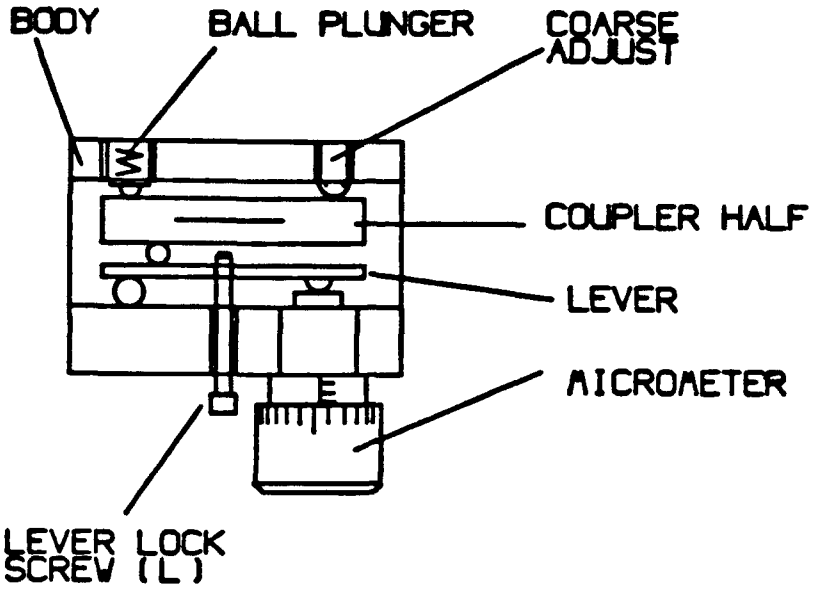

Figure 3-4
Schematic of the directional coupler package design.

To provide a tuning signal to drive the ring resonator, an electronic driving circuit was designed and fabricated. Figure 3-5 shows the drive circuit. Under a bias of ±12 V for circuits and a + 100 V for signal output, we were able to obtain a ramp voltage of nearly 100 V. This ramp voltage was used to monitor the finesse performance of the ring resonator. A detailed description of the ring performance is given in following related sections.

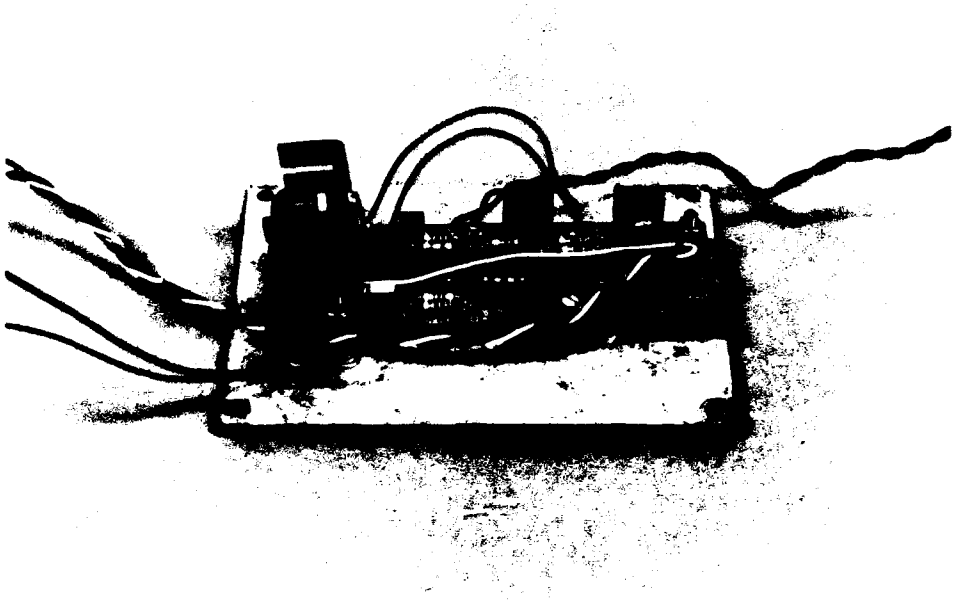

Figure 3-5
Picture of the piezoelectric driving circuit which provided a ramp driving signal.

3.1.2 Input Coupling and System Setup

To test the fiber-based ring resonator performance, two HeNe lasers were used. HeNe laser wavelengths were chosen because of their narrow linewidths, about 1 MHz. This choice satisfied the laser linewidth requirement discussed in Section 2.6. Figures 3-6 and 3-7 show the schematic and picture of the testing setup, respectively. A HeNe laser beam of 632.8 nm and a HeNe laser beam of 611.9 nm are both incident into the input fiber port A with the use of a beam combiner and microscope objective. Precise optical alignment is required to couple the free space laser beams into the single-mode optical fiber. Furthermore, laser beam polarization must be controlled to match the polarization requirement of the polarization-maintaining (PM) fiber. The introduction of the other polarization effects will cause unnecessary resonator noise. This effect will be discussed later.

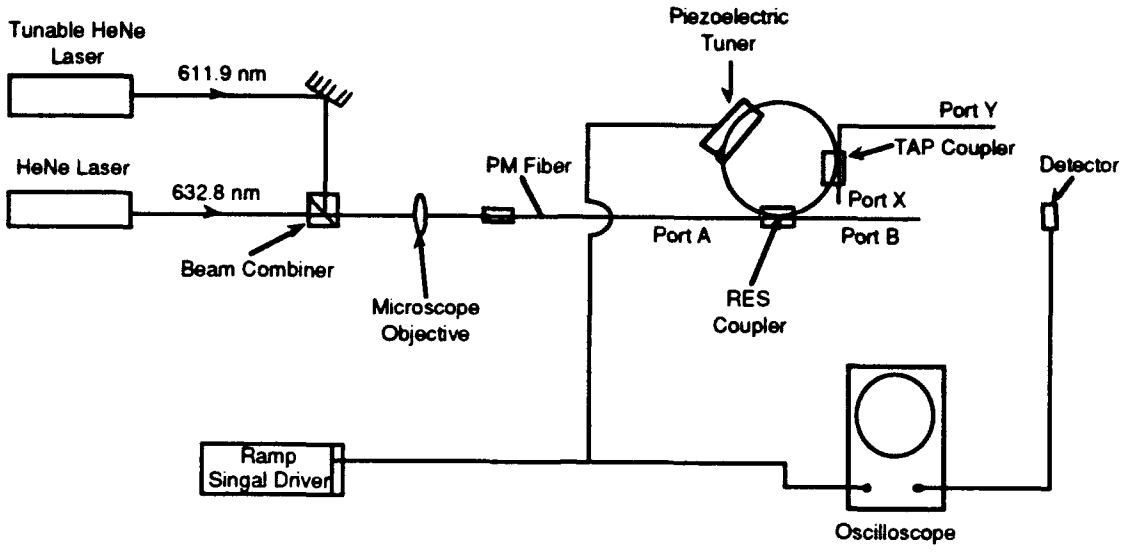

Figure 3-6
Schematic of the ring resonator testing setup.

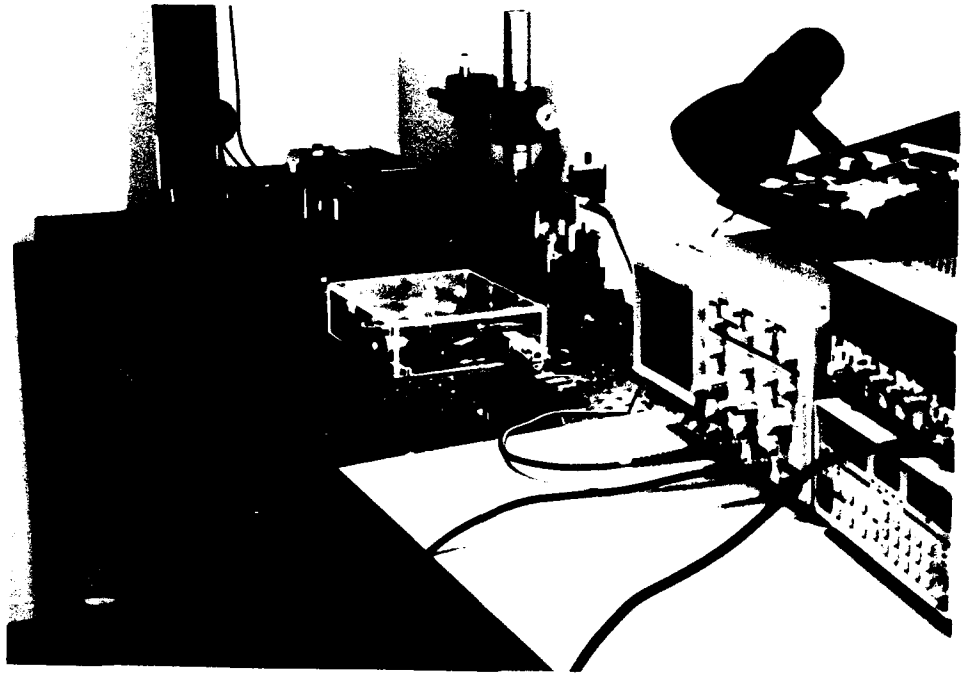

Figure 3-7
Picture of the fiber ring resonator testing setup.

3.1.3 Coupler Adjustment and Ring Resonance

When both couplers are in off coupling conditions, a bright throughput light is observed from the resonator output port B. Because of the nonresonance to the cross coupled resonator, the resonator acts like a single fiber connecting from port A to port B. When the RES coupler is adjust to the coupling condition, the resonance condition may be achieved for a specific laser wavelength under a fixed ring loop length or for a proper ring loop length under a fixed laser wavelength. To observe the resonant ring behavior, the ramp driving signal is introduced, which allows a continuous piezoelectric adjustment of the ring loop length (actually adjusting the optical path length).

Figure 3-8 shows the ring resonator throughput behavior at port B under a ramp piezoelectric driving control. The tap coupler is set off and one HeNe laser of 632.8 nm wavelength is turned on for this test. Under a proper voltage setting there is a significant energy loss on port B (a dip in the lower trace on Figure 3-8). When the resonant condition is reached, significant energy is coupled into the ring, continuously propagating in the ring (with little coupled back to port B). Loss in the ring is due to scattering and absorption. The repeat dip patterns correspond to the input laser wavelengths. The HeNe laser has multiple lasing lines. The four non-identical dips are caused by the corresponding laser lines. Therefore, measurements of actual ring behavior for a particular laser line must consider the repeated dip pattern.

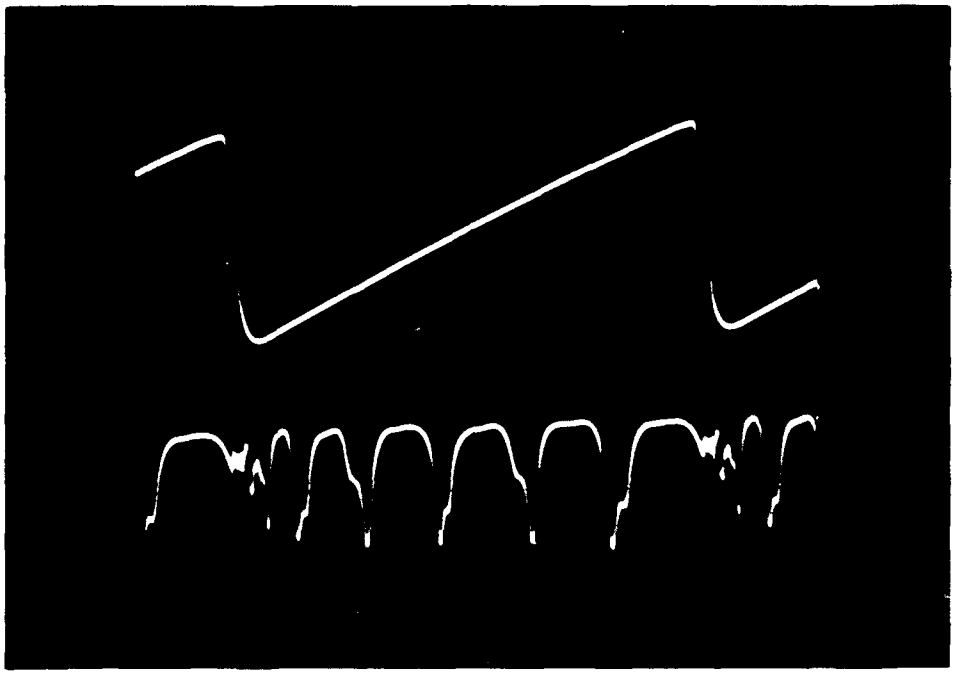

Figure 3-8
Performance of the ring resonance detected from port B
and seen on an oscilloscope under a ramp drive voltage bias.

Figure 3-9 shows a similar resonator response, but this time the adjustment is achieved through the input optical polarizer. Additional small dips observed are believed to be caused by the incorrect input polarization couplings since both TE and TM modes now exist in the ring resonator. This effect is obviously important and can be used to monitor the input polarization coupling status.

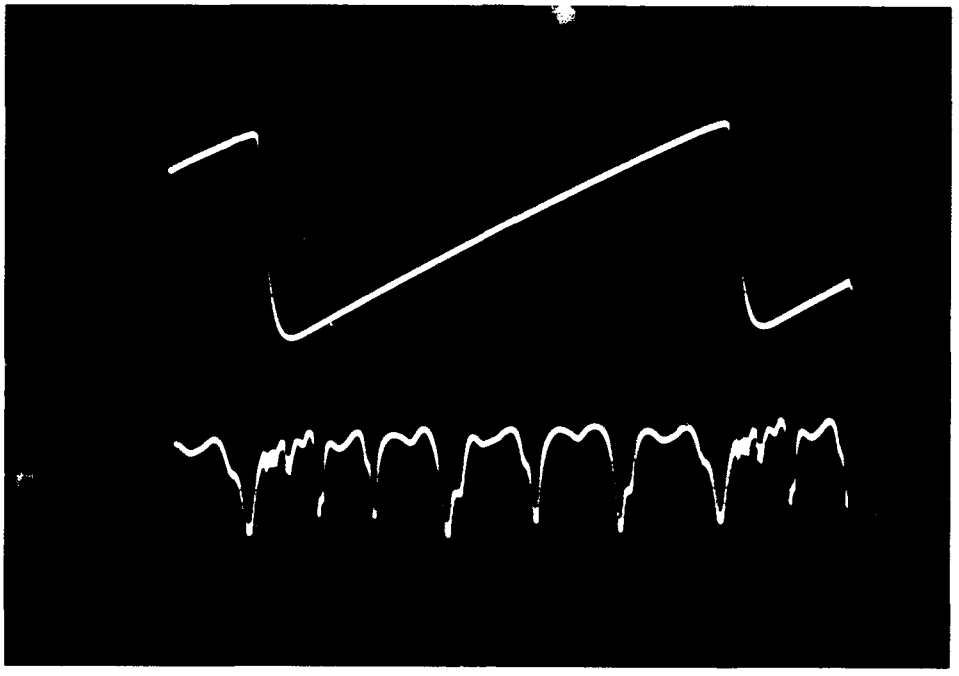

Figure 3-9
Performance of the ring resonator with incorrect polarization input.

3.1.4 Finesse and Selectivity

The sharp output resonator response under a ramp voltage bias shown above can be used to determine the resonator finesse. Since the finesse is defined as the free spectral range divided by the selectivity bandwidth, under a linear ramp voltage bias it is equivalent to the value determined from dividing the time spacing between two repeated dips by the bandwidth of the dip. Therefore, from Figure 3-8, we determined that the finesse of the ring resonator under zero tap coupling is 19. This value was measured to be about 40 before the device damage occurred during the optimization tuning. This value can in fact be as large as over 100, as tested at Canadian Instrument and Research, Ltd. before shipping. Based on the theory and other reported results [9], optimizing the device design and fabrication can provide a device finesse of over 1000 with no tap coupling.

The selectivity of the ring resonator is the bandwidth of the dip in a frequency scale. Therefore, it can not be found from the oscilloscope response. However, since the full ring size is known, the device FSR can be calculated with Eq. (17). For example, with the ring loop length of 23 cm and a fiber core index of about 1.46, the FSR of the ring is 892.77 MHz. Therefore, the selectivity of

the ring resonator, Δf, is 46.99 MHz (calculated by dividing the FSR by the measured finesse value). The calculated finesse can be as large as 155 under 97% input coupling and 1% coupler loss, with no tap coupling. The lower finesse in the present device is believed to be caused by an increase damage-induced coupler loss. When we simulated the experimental results, we found that the experimental results could match the theoretical ones under 85% input coupling, 5% input coupler loss, 0% tap coupling, and 10% tap coupling loss. This is very likely to occur since high coupler losses after damage is observable.

The above results are based on the optimized coupling at the RES coupler with the tap coupler set at zero. When the tap coupler is tuned on, which is necessary for the resonator to be used in the crossbar structure, the finesse and selectivity are expected to be reduced, as expected due to the increased ring loss from the tap coupler. Figure 3-10 shows the ring resonator response to ramp voltage bias as detected from port Y. The transmission response is similar to the two-mirror Fabry-Perot resonator and is as predicted in Figure 2-5. Similar calculation determined that the ring resonator finesse is 6, much lower than the measured value of 19, found earlier. The new frequency selectivity is 148.8 MHz. The laser linewidth has little effect to the new selectivity determination since the linewidth is about 1 MHz, much smaller than the previously determined selectivity bandwidth value. Again, these results were not optimized. Based on the results, as shown in Table 11 for the cross coupled ring resonator, optimizing the device fabrication by reducing the coupler loss can improve the device finesse and selectivity to 77.5 and 11.5 MHz, respectively. And, optimizing fabrication is possible with present technology.

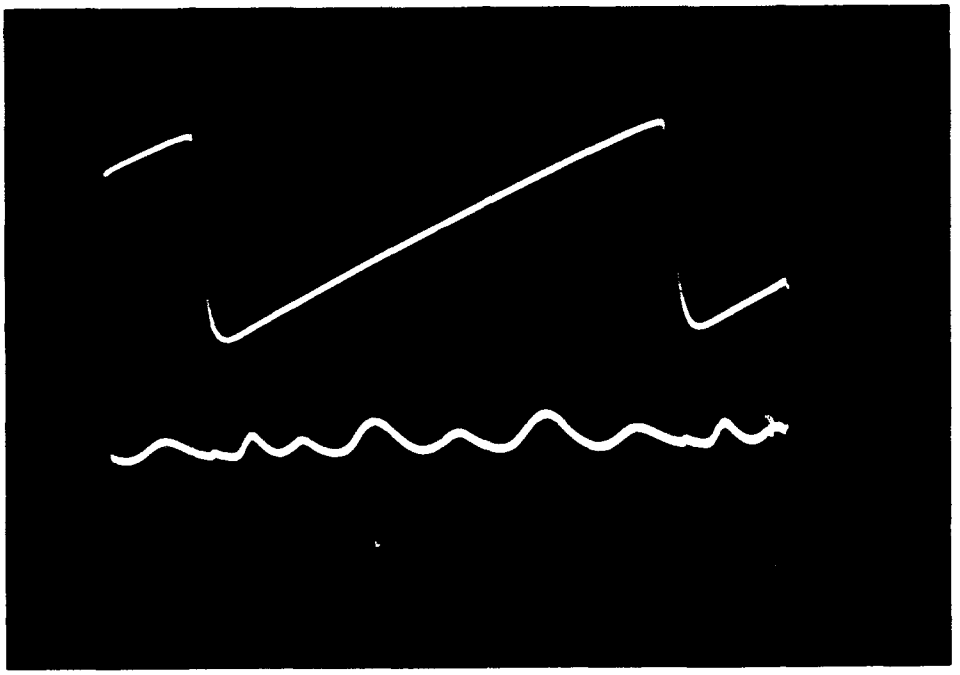

Figure 3-10
Ring resonator response as measured from port Y under a ramp voltage bias.

Table 11 Calculated Cross Coupled Ring Resonator Performance under 97% Input

C-Ring Resonator Calculation Results

Input Coupler Efficiency =	.97000
Input Coupler Loss =	.01000
Tap Coupler Efficiency =	.03000
Tap Coupler Loss =	.01000
Input To Tap Coupler Distance =	80.00000 mm
Tap To Input Coupler Distance =	150.00000 mm
Laser Wavelength =	632.80000 nm
Ring Propagation Loss =	- .200 dB/km
Refractive Index Of The Ring =	1.46000
Total Transmission =	.02656 %
Finesse =	77.53647
Maximum Transmission =	55.95244 %
Minimum Transmission =	.02295 %
Free Spectral Range =	892.770985 MHz
Frequency Bandwidth (FWHM) =	11.514207 MHz
Free Wavelength Range =	.0011925 nm
Wavelength Bandwidth (FWHM) =	.0000154 nm

3.1.5 Demonstration of Wavelength Selective Coupling

To demonstrate the wavelength selective coupling and switching effect, both HeNe lasers of 632.8 nm and 611.9 nm wavelengths were turned on. However, direct observation of the performance on oscilloscope was difficult since the 611.9 nm laser light is very weak. Only a small dip and peak are added to the response curves measured at port B and port Y, respectively. Figures 3-11 shows small dips observed at port B when 632.8 nm laser light was blocked. The dip location with respect to the ramp drive voltage can be compared to that of Figure 3-8. There are different dip locations for the 632.8 and 611.9 nm laser lines. Visual observation of the color change at port Y, under slow triangular swiping bias of about 1 Hz frequency, is much easier. DC bias at a proper voltage can fix the output Y at a particular wavelength but suppress the other wavelength output. This method was used to measured the throughput of the system and the signal crosstalk.

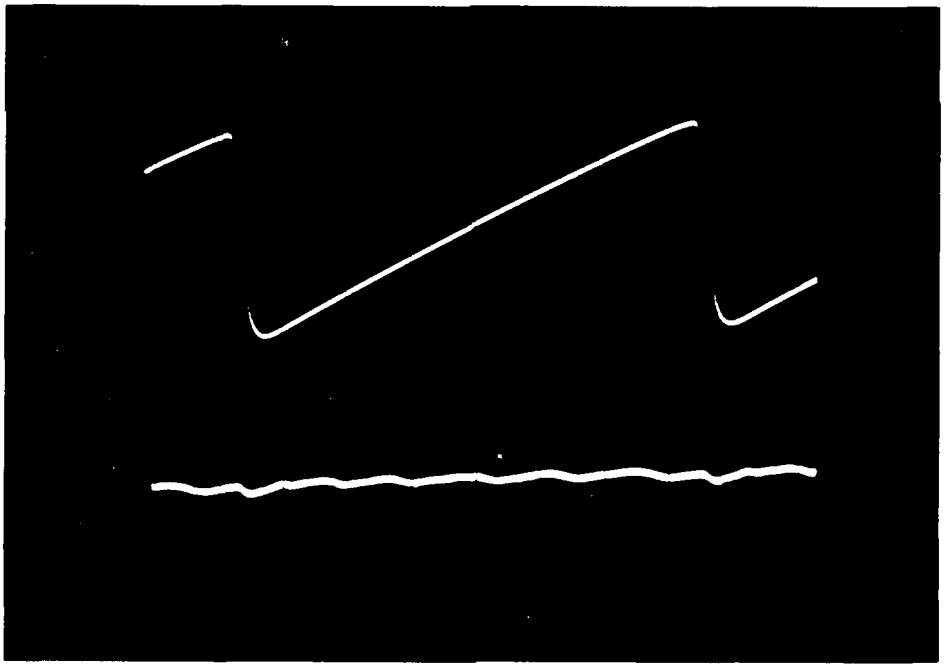

Figure 3-11
Transmission dips observed from port B for 611.9 nm laser line.
The location of dips are different than that of Figure 3-8 for 632.8 nm laser line.

3.1.6 Device Throughput and Crosstalk

To measure the device throughput, we first measured the input power to the fiber by monitoring the transmission power at port B when both RES and TAP couplers were set at zero coupling. Assuming the fiber propagation is negligible in the total 2 m propagation distance, which is in fact true based on -0.2 dB/km loss, we obtain the input power of 45 μW. When both couplers are set at the above resonance condition, we measured the maximum optical power at port Y to be ~16.2 μW under a optimum DC bias. Therefore, the system throughput for the present device and under the present coupling condition and bias setting is 16.2 μW/45 μW(100%): 36%. Optimizing the device can achieve a 56% throughput (see Table 11). The throughput efficiency can be increased to over 81% when input coupler efficiency drops to 90% and the tap coupler efficiency increases to 9%.

The crosstalk of the system is defined as the ratio of energy detected at the other wavelength's optimum bias to its own maximum transmission. For example, at the 632.8 nm laser wavelength, we measured the maximum optical power at port Y to be W1 under a optimum bias of V1. At 611.9 nm wavelength input we found that its maximum transmission at port Y occurred at bias V2. Therefore, if we detect an optical power of W2 at V2 for 632.8 nm wavelength, we can determine the system crosstalk to be

$$\text{Crosstalk} = -10 \times \text{Log}(W2/W1) \tag{35}$$

Based on this measurement principle, we found that the crosstalk of the present device is about -8 dB. Again, optimizing the device performance can result in less than -33.86 dB crosstalk based on the maximum and minimum transmissions shown in Table 11.

The crosstalk of the crossbar switch is independent of the crossbar size N. This aspect is an important advantage of our novel crossbar design.

3.1.7 Applicability to Fiber Ring Crossbar Structure

In principle, the fiber-based ring wavelength selective switch can be used for the demonstration of the fiber-based ring crossbar switch shown in Figure 1-1. Since each ring is to be biased and to operate on a specific wavelength, wavelength division multiplexing can be achieved from the input

set of ring switches. The multiplexed multi-wavelength beams can be demultiplexed at the output set of switches due to selective coupling from the trunk fiber to the output fibers. Thus, functional behavior of the crossbar is based on the known ring performance. The fabrication of such ring crossbar device is straightforward and is based on current fiber-based ring fabrication technology.

However, the present piezoelectric driving of the ring switch tuning has speed limitations. Typically, the piezoelectric driving device is limited to a few MHz. When this speed is acceptable for some applications, the piezoelectric-driven ring crossbar shown in Figure 1-1 can be easily commercialized. However, when the tuning speed is expected to be faster than several tens or several hundreds of MHz, an electro-optic tuning mechanism must be adopted. One approach for implementing electro-optic tuning is the use of waveguide-based ring technology. This approach, as discussed before, is high risk since the ring waveguide must be precisely designed and fabricated to lower its curvature or bending loss. Low-loss silica-on-silicon ring waveguides have been demonstrated with a finesse of more than 182. The thermal optic tuning speed on such waveguides is about 0.8 msec. The performance of low-loss ring waveguides on an electro-optic substrate such as $LiNbO_3$ has not yet been comparable with the silica-on-silicon technology. Because they are compact and can be easily fabricated in batches, electro-optic tunable waveguide-based ring crossbars should be considered for research and development. The present choice for demonstrating high-speed ring crossbar tuning for near-term commercialization purposes is the fiber-based ring resonator in conjunction with a fiber pigtailed low-loss waveguide phase modulator, illustrated in Figure 2-8. Enhanced pigtailing techniques, in conjunction with the above fiber-based ring switch, will be considered in Phase II to create a 4 x 4 working crossbar device. Another choice for Phase II development is to utilize silica-on-silicon waveguide technology, with the recently reported electro-optic effect, on a silicon substrate for tuning. The Phase II research direction will be discussed in the Phase II proposal.

3.2 Demonstration of Fiber/Waveguide Pigtailing for Channel Waveguide Phase Modulator

3.2.1 Fabrication of Channel Waveguide on X-cut $LiNbO_3$ Substrates

Since a polarization-maintaining fiber will be used in the construction of the fiber-based ring resonator switch, a highly polarization-selective waveguide phase modulator is preferred. We selected a proton exchange technique on X-cut $LiNbO_3$ substrate to achieve a waveguide that can support only a single TE mode. Proton exchange in $LiNbO_3$ involves the replacement of lithium

with hydrogen. It takes place when the substrate is immersed in a proton source, i.e., an acid or a dydrate melt at an appropriate temperature. Among the many media that can be hydrogen sources for proton exchange, benzoic acid is the most common because of its high boiling point (249°C), stability throughout its liquid phase, low toxicity, and low cost. A high boiling point enables proton exchange to occur at high temperature, which makes diffusion faster and improves the stability of the exchanged compound, which in turn makes the exchange results, or waveguide parameters, more consistent.

Through the proton exchange in benzoic acid, the extraordinary index, n_e, is increased by approximately 0.12 [13], and the ordinary index, n_o, is decreased by approximately 0.05 [14] at an optical wavelength of 632.8 nm. Because of the large change in the extraordinary index, a much smaller channel depth to channel width ratio is required in a waveguide channel that supports only single-mode propagation. For example, for a 4 μm width single-mode channel, the depth is only about 0.26 μm, as calculated using Marcatilli's method [15]. In these circumstances, the non-uniform side-wave diffusion during proton exchange can be neglected, and thus a channel of rectangular shape can be expected. The masking material affecting the proton exchange [16] can also be neglected, due to the much larger channel width compared to the channel depth. In our experiment, we chose an X-cut $LiNbO_3$ substrate because of its much lower susceptibility to surface damage (during proton exchange) than that of Y-cut $LiNbO_3$ [17]. A high polarization extinction ratio, of 60 dB, can be expected from the proton exchanged waveguide [18].

In order to effectively utilize the large index change in n_e for waveguide formation, we chose X-cut $LiNbO_3$ with a channel waveguide orientation along the y-direction. The waveguide fabrication processes are illustrated in Figure 3-13. To prevent thermal shock, cleaned substrates that had a Cr/Al lift-off mask with openings for the channel regions for proton exchange were pre-heated up to the exchange temperature. The sample was then slowly immersed in molten benzoic acid, which included 1 Mol% of lithium benzoate. Lithium benzoate reduced the exchange speed, enabling better control of exchange depth and reduction of waveguide propagation loss by reducing the generation of stress-induced voids in the fast exchange process. Using this fabrication process we successfully fabricated a single-mode channel waveguide.

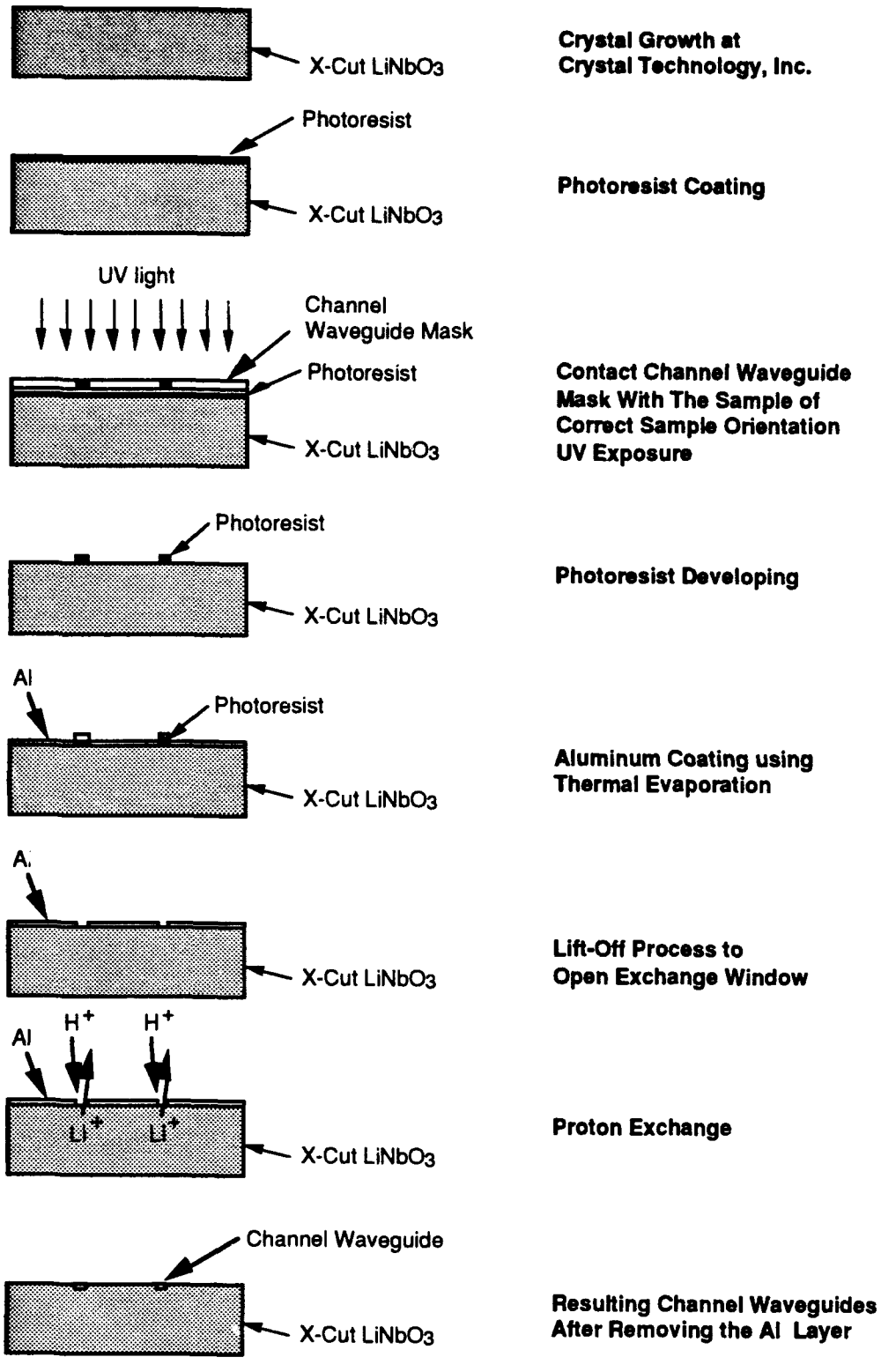

Figure 3-13
Process for channel waveguide fabrication on an X-cut $LiNbO_3$ substrate.

3.2.2 Device End-Face Polishing

To facilitate the device edge coupling and fiber pigtailing, necessary for the integration of the fiber-based ring resonator with the waveguide phase modulator and to provide high speed tuning, the channel waveguide phase modulator's end faces must be polished to optical quality. We performed this device end face cutting and polishing. The polished devices were tested with a HeNe laser at a wavelength of 632.8 nm. The incident laser beam was first focused by a 20x microscope objective. The focused beam at its beam waist is incident on one end of a polished channel waveguide. A sizable portion of the laser energy was thus coupled into the channel waveguide and exited at the other end of the device, where another microscope objective placed near the device end functioned as an imaging lens (see Figure 3-14). The near-field image of the output device was found on a screen. Figure 3-15 shows a photograph of this near-field image. A bright spot located at the center of the picture designates the channel throughput light; the upper and lower background light is the uncoupled portion of the incident beam in air and substrate, respectively. These background lights can help determine if the proper coupling is achieved. The bright spot can help determine if proper end face polishing is achieved. In addition, by observing the near-field and far-field radiation pattern of the channel waveguide mode, we can determine whether the device is single-mode or multi-mode device. Single-mode devices are required in the phase modulator to allow precise control of the ring resonator performance. After good device end-face is obtained, the device is ready for further processes including electrode deposition and fiber/waveguide pigtailing.

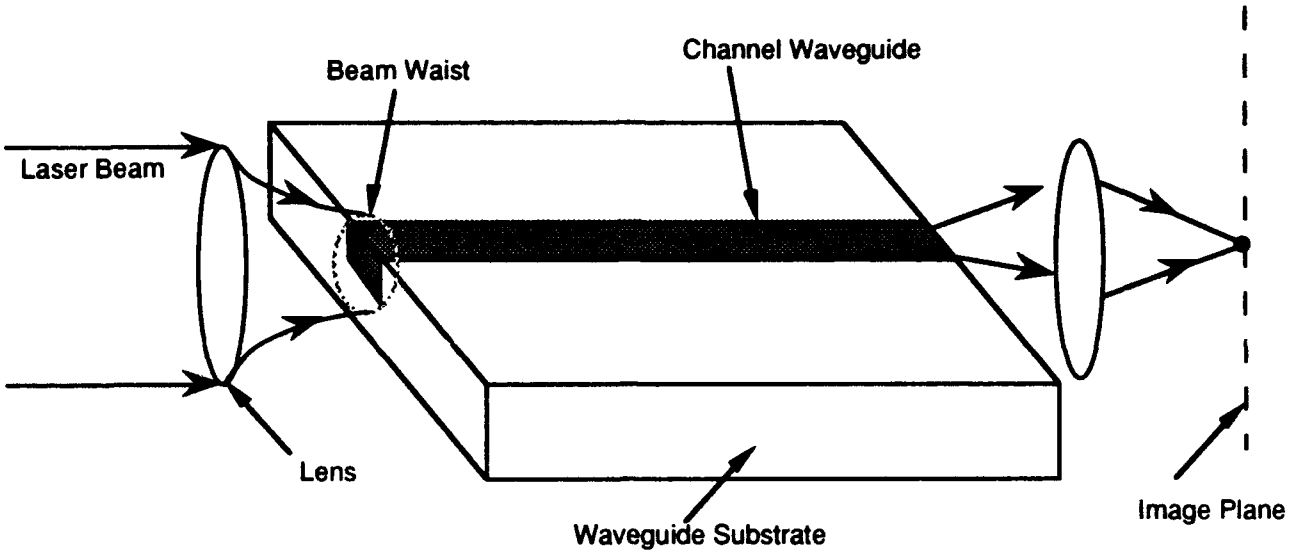

Figure 3-14
Schematic of end-fire coupling for channel waveguide testing.

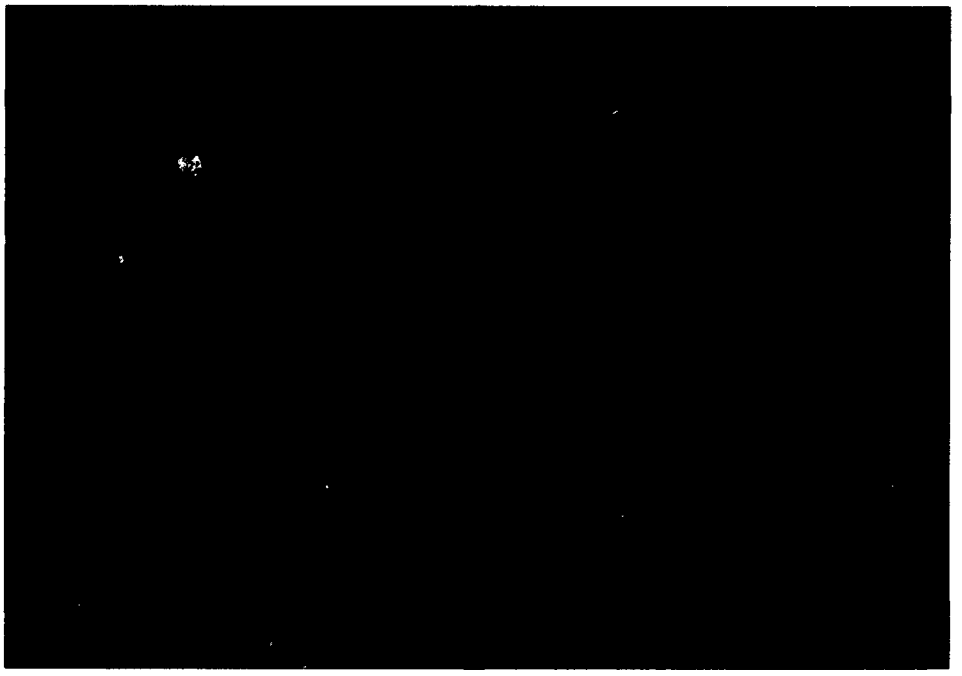

Figure 3-15
Near-field image of the channel waveguide throughput.

3.2.3 Electrode Deposition

Figure 3-16 shows the cross-sectional view of the electrode pattern we desired to provide the required E_z tuning field.

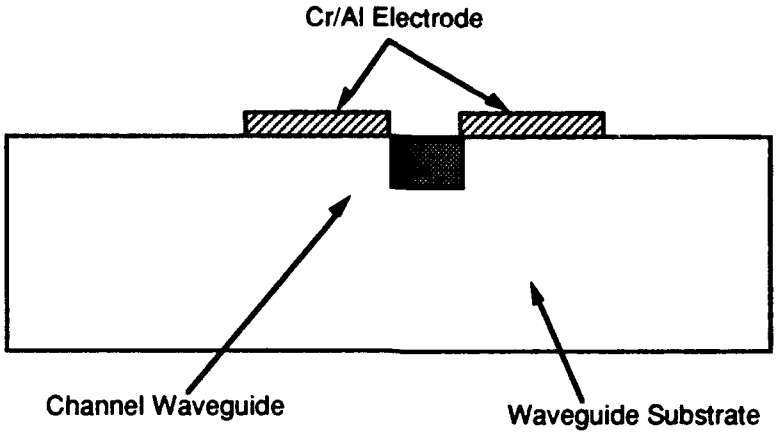

Figure 3-16
Cross-sectional view of the electrodes on channel waveguides.

Typically, the electrodes used in conventional electro-optic modulators are made of Cr/Al or Pt/Au realized by thermal evaporation or sputtering. In this experiment, Cr/Al electrodes were chosen due to the ease of thermal evaporation and their low cost. The fabrication process for the Cr/Al electrodes on $LiNbO_3$ substrate is illustrated in Figure 3-17. The experimental procedures involve sample surface cleaning in a cleanroom environment, photoresist spin coating, a baking treatment, contact printing of the electrode pattern from the mask onto the channel waveguide sample with alignment of sub-micron accuracy, photoresist developing, Cr/Al metal deposition, and lift-off processing.

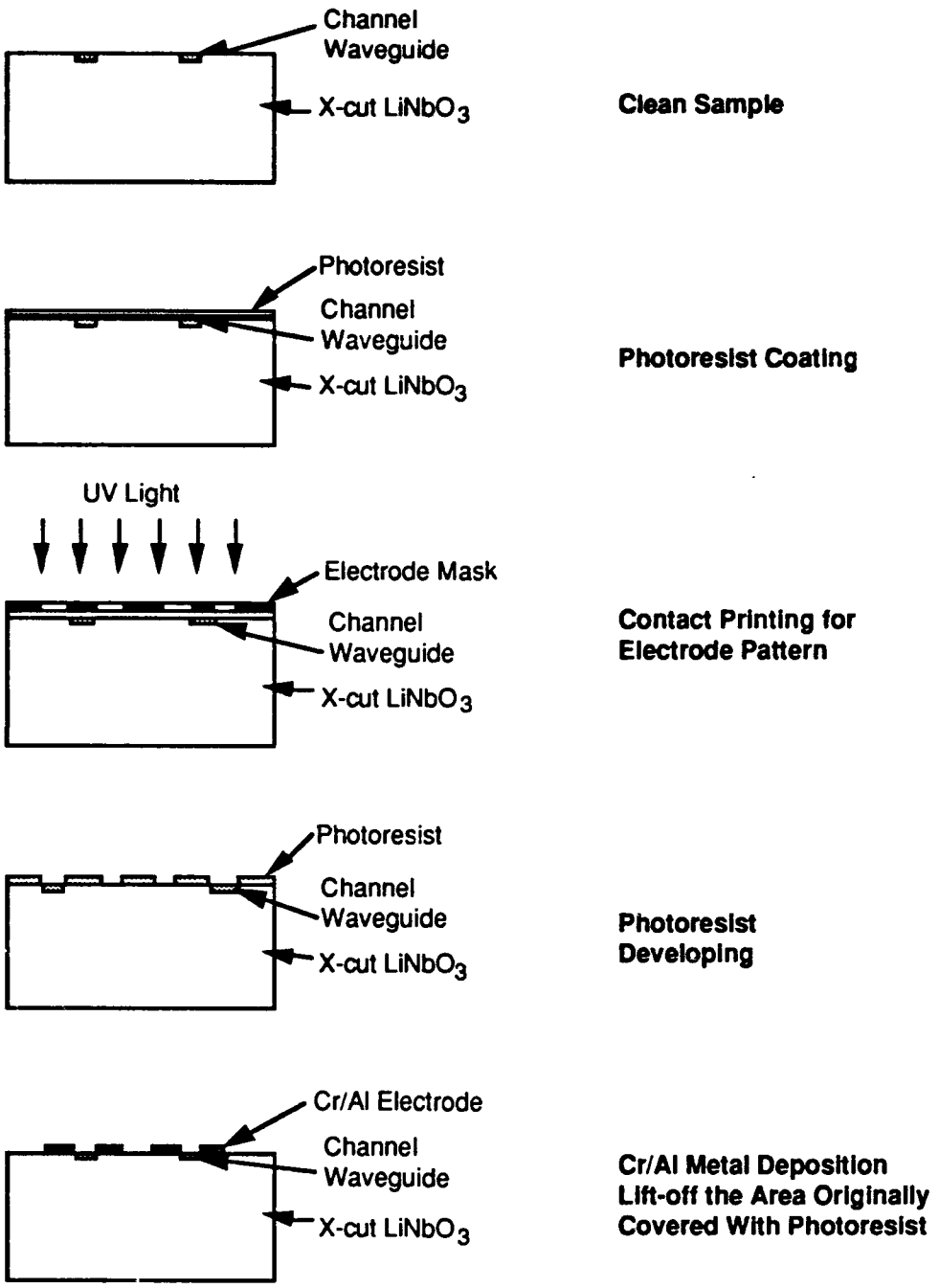

Figure 3-17
Fabrication process for electrode pattern deposition on a channel waveguide sample.

3.2.4 Phase Modulator Prototype

Following the waveguide and electrode fabrication, the sample was mounted on a piece of glass substrate for easier handling. The substrate could be any material that can hold the optical fiber-based ring resonator. Bonding wire connects the modulation electrode to the driving circuit. The performance of our packaged phase modulator prototype can then be tested by observing beam interference effects with a reference beam. During earlier research, sponsored by SDIO, successful phase modulation had been observed through a Fabry-Perot cavity [19]. Therefore, successful phase modulation is anticipated even though the modulation test was not performed on our current device due to limited Phase I time. Device parameters are summarized in Table 12.

Table 12 Device Parameters for the Waveguide Phase Modulator Prototype.

Electro-optic Substrate	X-cut $LiNbO_3$
Waveguide Fabrication	Proton Exchange
Exchange Solution	Benzoic Acid with 1 Mol% Lithium Benzoate
Exchange Temperature	200°C
Channel Waveguide Mode	TE
Channel Waveguide Orientation	Y-Axis
Channel Waveguide Width	~ 5 μm
Electrode Material	Cr/Al
Electrode Gap	8 μm
Electrode Width	5.5 mm
Electrode Length	2.8 mm
Capacitance	~4 pF
Waveguide Propagation Loss	< -0.4 dB/cm
Device Length	6 mm
Device End-Face Polishing	Yes
Device End-Face Coating	None
Anticipated Modulation Bandwidth	~1.6 GHz

For the current device, DC bias electrode was not incorporated. An old electrode mask was used for the fabrication demonstration due to limited Phase I budget. In the crossbar system, both DC and RF bias electrode patterns will be incorporated within the same phase modulator. DC bias can be used for initial bias and for temperature compensation, along with a temperature compensation circuit. RF bias can be used to provide actual wavelength selective tuning of the ring resonator.

3.2.5 Demonstration of Fiber/Waveguide Pigtailing for the Phase Modulator

A waveguide electro-optic phase modulator is a high-speed device with reported modulation speed exceeding several tens GHz. By pigtailing the waveguide phase modulator into the fiber ring, a high-speed ring resonator switch can be realized. Figure 2-8 shows the pigtailed waveguide phase modulators in the ring crossbar switch structure. Since the resonator is sensitive to the total ring loss, low-loss pigtailing from fiber to waveguide to fiber is essential for the high-performance ring switch and crossbar.

Demonstrating fiber/waveguide pigtailing is an important goal of Phase I. This demonstration shows that the implementation of the waveguide phase modulator with fiber-based ring resonator is feasible for a crossbar demonstration.

To fiber pigtail the single-mode waveguide, a glass waveguide holder was fabricated first. Single-mode glass fibers with core diameter of 5 μm and clading diameter of 125 μm were used for pigtailing. Fiber ends were cleaved and inserted into capillary tubes for polishing. Then, the fibers, the waveguide holder, and the single-mode waveguide were mounted on a precision optical alignment stage. The pigtailing setup is shown in Figure 3-18. HeNe laser light with a 632.8 nm wavelength was fed into the fiber for optical alignment. With proper alignment of sub-micron alignment accuracy, optimum optical coupling was achieved. UV epoxy was then used to hold the fibers, the waveguide, and the holder together to maintain the optimum input/output optical coupling condition. The final pigtailed device is shown in Figure 3-19.

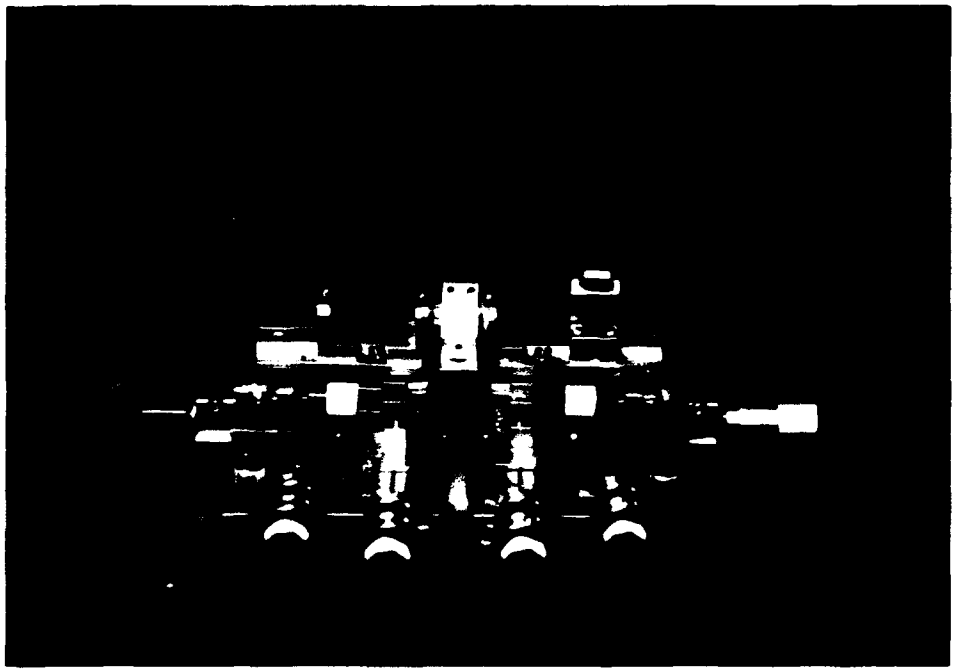

Figure 3-18
Fiber/waveguide pigtailing setup using high precision optical alignment stages.

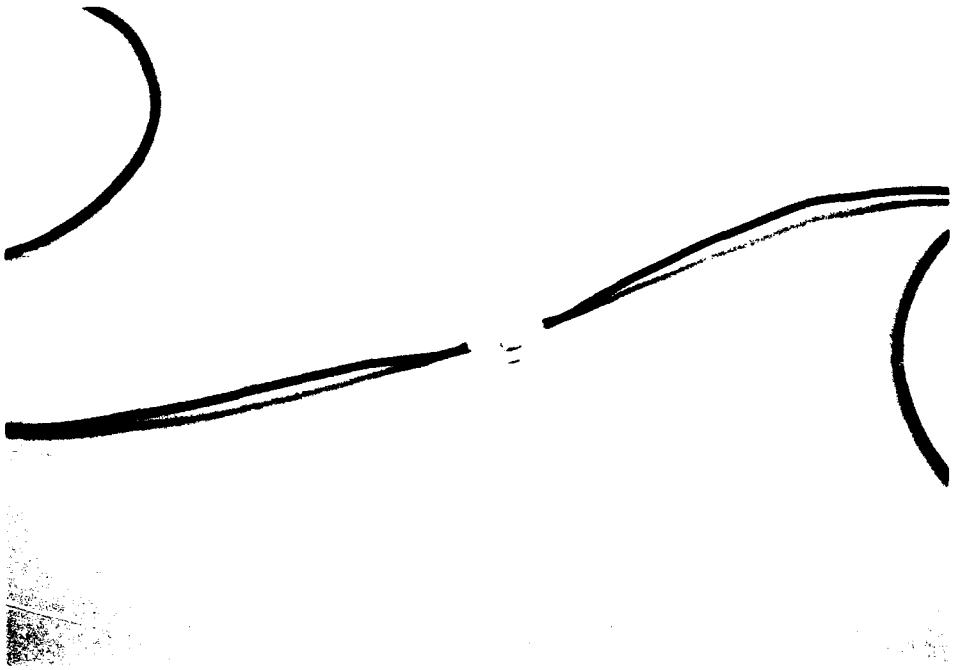

Figure 3-19
Picture of a fiber pigtailed waveguide phase modulator.

To evaluate the fiber pigtail device, the HeNe laser beam was again fed into the input fiber. The optical power from the output fiber was measured. The fiber-to-fiber insertion loss was measured by comparing the input and output optical powers. For the present device the insertion loss was determined to be nearly -11 dB. Partial loss is due to the polarization mismatch between fiber and waveguide. A regular fiber of circular cross section (not a polarization-maintaining fiber) was used and -3 dB loss resulted from 50% coupling loss due to a polarization mismatch to the TE mode only waveguide. Therefore, the effective pigtailing loss for a TE polarized beam is -8 dB. This loss is considered large compared to the commercial-repeatable pigtailing loss of -3 to -4 dB. However, as the first fiber pigtailed waveguide device created at POC, the result is considered satisfactory.

Possible causes and solutions for the high pigtailing loss are shown in Table 12 .

Table 12 Cause of Pigtailing Loss and Optimization Solution

CAUSE	SOLUTION
There is a mode profile mismatch between fiber and waveguide mode. The fiber core diameter is 5 μm while the waveguide dimension is about 4 μm by 0.3 μm.	Optimization of the waveguide mode to better match with fiber mode can be performed by thermal annealing process.
There is polarization mismatch.	The polarization mismatch problem can be solved by using the desired polarization maintaining fiber with polarization alignment to TE mode only wave-guide.
The fiber and waveguide orientation may have slight angular misalignment mostly caused by the slightly tilted waveguide endface polishing with respect to channel waveguide orientation.	Handling with extreme care should avoid the problem.
The UV epoxy curing may result in some strain that shift slightly the fiber position and affect the optimum fiber/waveguide alignment.	Low stress and low shrinkage cement from EASTMAN Laboratory is a potential candidate to replace the UV epoxy.

These engineering solutions for optimizing the fiber/waveguide pigtailing can be addressed in a relatively straightforward manner, but not within the time frame of the Phase I. We will optimize the pigtailing process in Phase II if such a device structure is used so as to reduce the fiber/waveguide pigtailing loss to about -1 dB with polarization-maintaining fiber.

3.3 Advantages of the Ring Resonator Based Crossbar Switch Structure

The major advantages of the crossbar switch structure are:

1. New wavelength-based crossbar principle.

2. The signal crosstalk level can be lower than -30 dB and the crosstalk is independent of N.

3. Our N x N crossbar uses only 2N switching elements, compared to N^2 switching elements in conventional crossbars.

4. Lower power consumption because of fewer switches.

5. Easy switching pattern reconfiguration due to simple switching pattern. The change of one pathway may not affect other pathways.

6. High-speed switch reconfiguration (> GHz) when waveguide phase modulators are used.

7. One-to-many fanout capability without using additional fanout circuits.

8. High switching contrast ratio (over 1000:1).

9. Mature fiber pigtailing technology for fiber-based ring and waveguide modulator integration.

10. Thermal expansion and contraction and other environmental effects can be compensated by electronic feedback switching bias.

11. The number crossbar switching array elements can be ten times the present crossbar technology, depending on the finesse of the ring resonator.

12. The crossbar device can be readily used as an active wavelength division multiplexer and demultiplexer.

13. The new crossbar structure is anticipated to reduce electromagnetic cross-coupling due to reducing switch number N^2 to 2N for N x N crossbar.

14. The fiber-based crossbar when developed can readily be implemented in fiber communication and switching networks. Therefore, its near-term commercialization is possible.

15. Monolithic integratability with other integrated optical and electronic components when waveguide ring device is used.

16. The waveguide-based ring crossbar device can be rugged packaged for high g environment.

4.0 POTENTIAL APPLICATIONS

The new crossbar switch design with 2N switches, rather than N^2 switches, for an N x N crossbar with potential ten times larger switching array than in the conventional approach, can satisfy the requirements for reconfigurable large-scale data switching and optical computing. The crossbar switch when developed in Phase II can readily be used as an active wavelength division multiplexer (see Figure 4-1) and demultiplexer (a reverse arrangement of Figure 4-1). The wavelength separation between WDM channels does not have to be limited within a free spectral range or free wavelength range. Owing to the resonance effect that can occur on different mode numbers, the wavelength separation can range from 10^{-4} Å to over 10 nm depending on application. However, in choosing wavelength sets, the overlap of their transmission under the same bias voltage or choosing a set of (m,λ) to satisfy the Eq. (34) at the same bias or Δn, must be avoided.

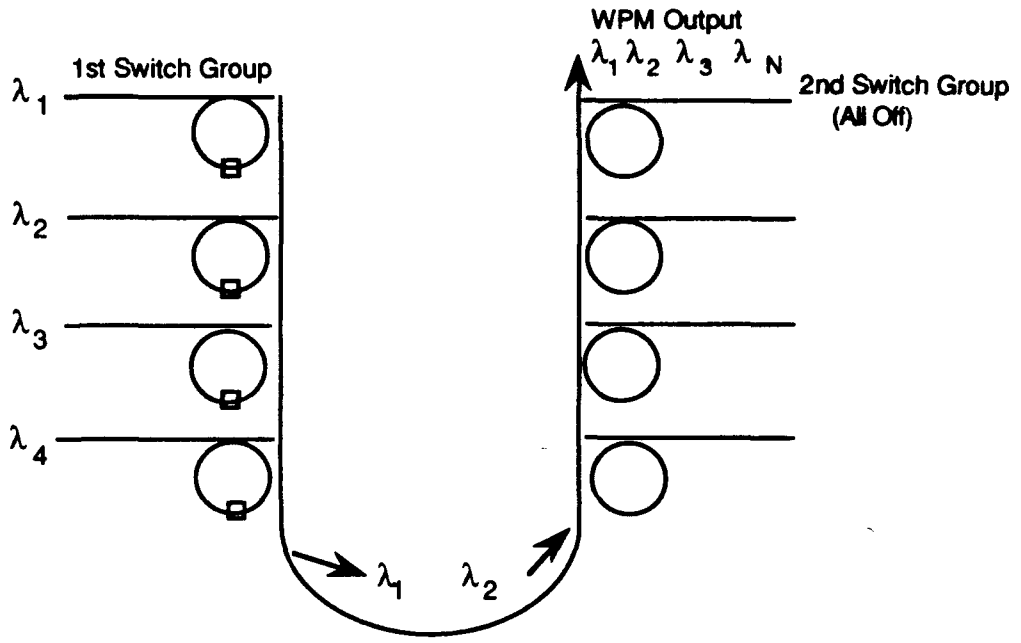

Figure 4-1
The crossbar switch can be used as active WDM device.

The fiber-based ring crossbar switch can be used in fiber communication networks without additional constrains. It can also be used in free-space opticai computing systems, for example, those that employ spatial light modulators. The waveguide-based ring crossbar switch, when developed, can be very compact and can be monolithically integrated with other optical and electronic microcircuit components to form a compact optical computing and data processing chip. It can also be fiber pigtailed for use in fiber optic communication applications. The proposed crossbar concept with its high reconfiguration rate is attractive and in some cases can replace other crossbars in the commercial market.

In addition to the above WDM and data switching applications, the developed crossbar can be used for active wavelength filters, multi-level 1 to M switching (see Figure 4-2), phased array antenna applications with multi-level switching, environmental sensing using an array of different ring sizes, multi-level logic (Figure 4-3), and signal quantization in the wavelength domain (Figure 4-4).

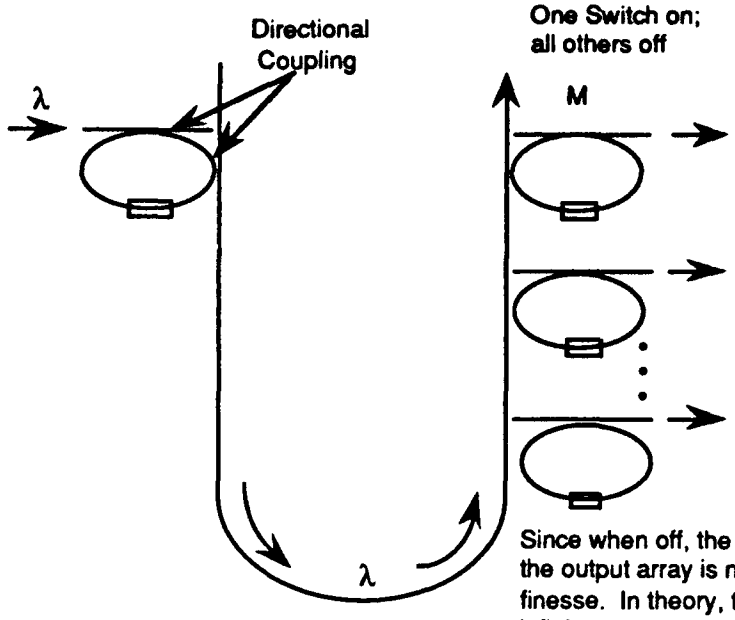

Since when off, the bias can be the same, the output array is not limited by device finesse. In theory, the M output can be infinity.

Figure 4-2
Multi-level switching (1 to M).

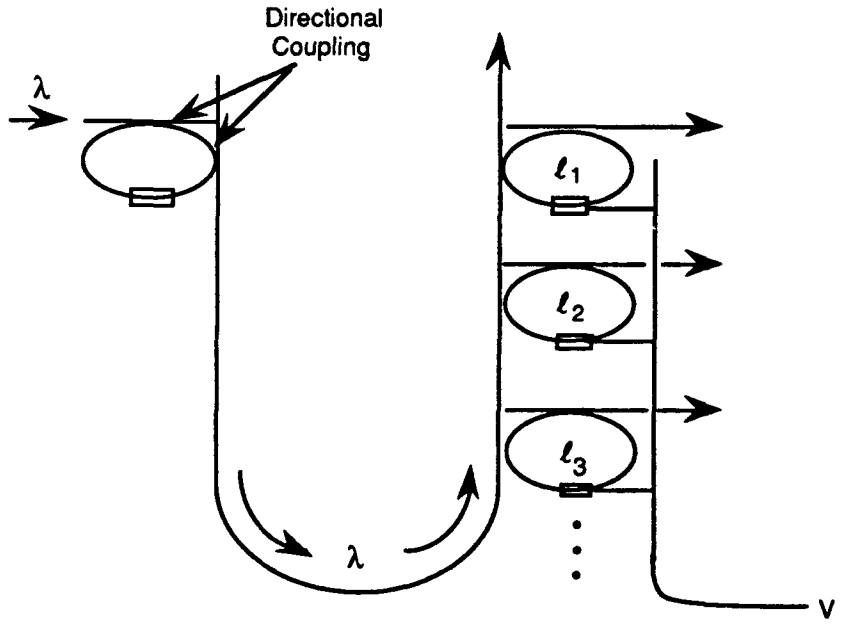

Figure 4-3
Multi-Level logic. When the tuning bias electrodes, ℓ_1, ℓ_2, ℓ_3,..., are slightly different in value, an analog voltage V can be converted to a specific output channel throughput. For example, at V_3, output channel 3 is on and all other channels are off. Such a conversion performs the signal quantization function.

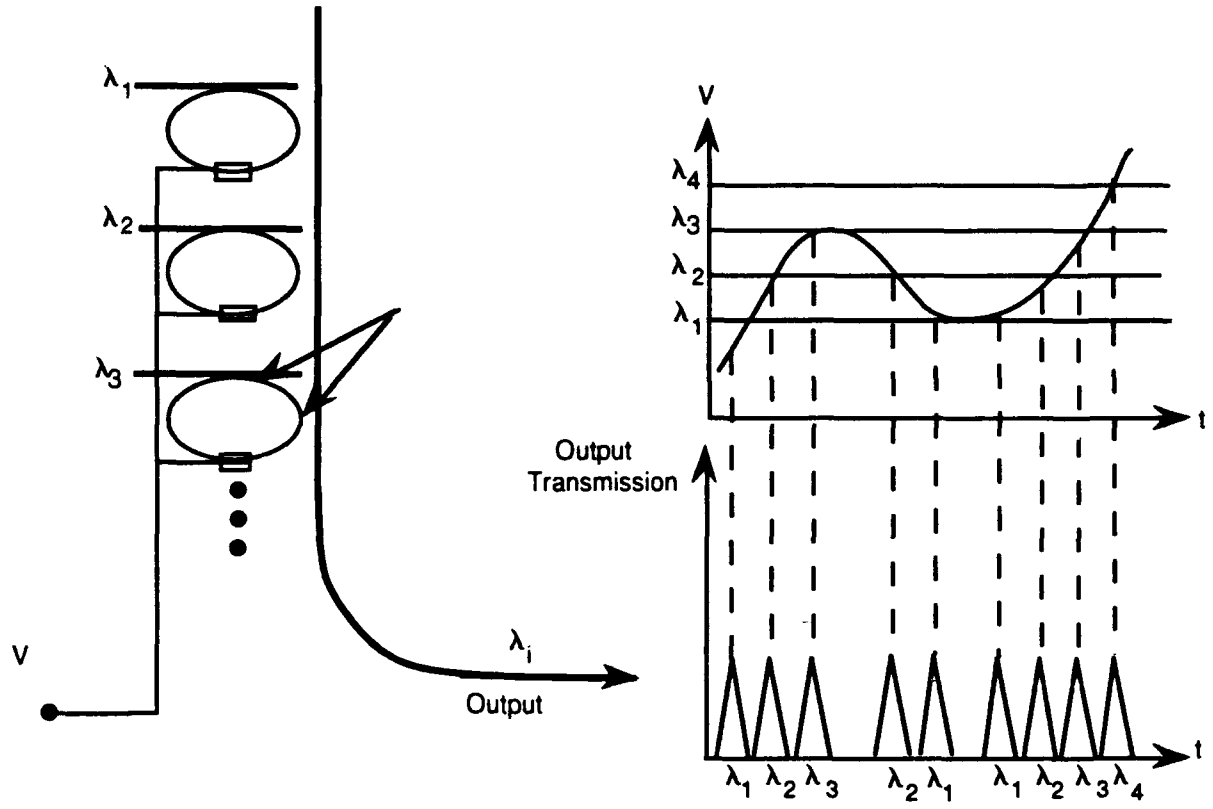

Figure 4-4
Signal quantization in the wavelength domain.

5.0 CONCLUSIONS

Physical Optics Corporation proposed a novel device structure for an optical crossbar based on a multi-wavelength ring resonator tuning/switching concept. In the Phase I program, we designed, analyzed, and demonstrated a basic ring resonator tuning/switching element to prove the feasibility of the crossbar concept. First, the working principle for the ring resonator switch was analyzed, theoretically. Then, design issues were addressed. Two approaches for the ring resonator tuning were identified: fiber-based ring resonator and waveguide-based ring resonator. The waveguide-based approach has the advantage of compact packaging and a low-cost batch fabrication potential. However, the present fabrication technology limits the ease of demonstrating a low-loss waveguide-based ring with a small bending radius on an electro-optic substrate. The fiber-based approach has the advantage of near-term commercialization based on a maturely developed fiber directional coupler technology. However, the ring size is relatively large and the device is bulky. The fiber-based approach by itself can be tuned by either a thermal or a piezoelectric driving source but is limited in tuning or crossbar reconfiguration speeds up to a few

MHz. A modified fiber-based ring crossbar structure has been identified that will increase its tuning/switching speed by implementing the device with fiber pigtailed waveguide electro-optic phase modulators. Based on such considerations, the simplicity of the crossbar demonstration, and the near-term commercialization possibilities, we chose the fiber-based ring device the crossbar switch design for the Phase I feasibility study. In the Phase II 4 x 4 crossbar switch development, both fiber and waveguide ring structures may be considered.

To demonstrate the feasibility of the fiber-based ring crossbar concept, a fiber-based ring resonator with both input and tap couplers was fabricated. The fiber-based ring device is based on single-mode polarization-maintaining fiber and directional coupler for input and tap couplings. The ring loop length is approximately 23 cm and the piezoelectric tuner is approximately 3.8 cm in length. The driving circuit used to provide nearly 100 V of ramp voltage was also designed and fabricated. At the HeNe laser wavelengths of 632.8 and 611.9 nm the fiber-based ring resonator has demonstrated the desired wavelength selective switching operation with device finesse of about 19 under zero tap coupling and 6 with some tap coupling. The non-optimized fiber-based ring device is capable of providing over 36% throughput with a potential of over 80% throughput efficiency. The resonator crosstalk is measured to be -8 dB with a potential of over -33.86 dB. Optimizing the device is possible by reducing the coupler substrate radiation loss, which is high in the present device due to fabrication defects. Also, a proton-exchanged channel waveguide was fabricated with polished device end faces. A fiber/waveguide pigtailing experiment was conducted during Phase I to show the capability of such pigtailing methodology at our facilities. The demonstrated efforts in both the fiber-based resonator switch and fiber/waveguide pigtailing can be used in Phase II to realize an optimized 4 x 4 ring resonator based crossbar switch.

The successful demonstration of the ring resonator switch and the ring based crossbar device can result in a number of applications. A potential application of the new crossbar is its use as an active wavelength division multiplexer and demultiplexer. The crossbar can also be used as an active wavelength filter, for multi-level switching, phased array antenna applications, environmental sensing, multilevel logic and signal quantization. Other applications in high-speed data switching, computing, and fiber communication can also benefit from the high reconfiguration rate and dynamics of the crossbar design.

6.0 REFERENCES

1. A. R. Dias, et al, "Fiber-Optic Crossbar Switch With Broadcast Capability," SPIE 825, 170 (1987).

2. R. C. Alferness, "Waveguide Electro-Optic Switching Arrays," IEEE J. on Selected Area in Communications, Vol. 6, 1117 (1988).

3. A. A. Sawchuck, B. K. Jenkins, C. S. Raghavendra, and A. Varma, "Optical Crossbar Networks," Computer, 50-60, (June 1986).

4. P. Granestrand, et al, "Strictly Nonblocking 8 x 8 Integrated Optical Switch Matrix," Electron. Lett., 22, 816 (1986).

5. J. B. D. Soole, K. R. Poguntke, A. Scherer, H. P. Leblanc, et al. "Wavelength-Selectable Laser Emission From A Multistripe Array Grating Integrated Cavity Laser," Appl. Phys. Lett., 61(23), 2750-2752 (1992).

6. K. Oda, N. Takato, and H. Toba, "A wide-FSR waveguide double-ring resonator for optical FDM transmission systems," J. Lightwave Technol., 9(6), 728-736 (1991).

7. P. Urquhart, "Compound Optical-Fiber-Based Resonators," J. Opt. Soc. Am. A, 5(6), 803-812 (1988).

8. L. F. Stolkes, M. Chodorow, and H. J. Shaw, "All-Single-Mode Fiber Resonator," Opt. Lett., 7(6), 288 (1982).

9. C. Y. Yue, J. D. Peng, Y. B. Liao, and B. K. Zhou, "Fiber ring resonator with Finesse of 1260," Electron. Lett., 24(10), 622-623 (1988).

10. R. Adar, Y. Shani, C. H. Henry, R. C. Kistler, G. E. Blonder, and N. A. Olsson, "Measurement of very low-loss silica on silicon waveguides with a ring resonator," Appl. Phys. Lett., 58(5), 444-445 (1991).

11. E. A. J. Marcatili, "Bends in optical dielectric guides," Bell System Technol. J. 48, 2103-2132 (1969).

12. S. Cao, "Waveguide ring resonator on LiNbO3", sponsored by Harris Corporation, (Private communication).

13. J. L. Jackel, C. E. Rice, and J. J. Veselka, "Proton Exchange for High-Index Waveguides in LiNbO3," Appl. Phys. Lett., 41, 607 (1982).

14. J. L. Jackel, C. E. Rice, and J. J. Veselka, "Proton Exchange in LiNbO3," ferroelectrics, 50, 165 (1983).

15. E. A. J. Marcatili, "Dielectric Rectangular Waveguide and Directional Coupler for Integrated Optics," The Bell System Technical Journal, p. 2071 (1969).

16. N. A. Sanford, W. E. Lee, "Analysis of Proton Exchanged Channel Waveguides in LiNbO3," Proc. SPIE, 578, 7 (1985).

17. M. Goodwin and C. Stewart, "Proton-Exchanged Optical Waveguides in Y-cut Lithium Niobate," Electron. Lett., 19, 223 (1983).

18. P. G. Suchoski, T. K. Findakly, and F. J. Leonberger, "Stable Low-Loss Proton-Exchanged LiNbO3 Waveguide Devices with No Electro-Optic Degradation," Opt. Lett., 13, 1050 (1988).

19. Michael R. Wang, Tomasz Jannson, and Vladimir Katsman, "A Novel Coding Technique for the Implementation of An Electrooptic Analog-to-Digital Converter," Proc. SPIE, Vol. 1849, (1993).